We are IntechOpen,
the world's leading publisher of
Open Access books
Built by scientists, for scientists

4,800
Open access books available

122,000
International authors and editors

135M
Downloads

Our authors are among the

154
Countries delivered to

TOP 1%
most cited scientists

12.2%
Contributors from top 500 universities

CLARIVATE ANALYTICS
BOOK CITATION INDEX
INDEXED

WEB OF SCIENCE™

Selection of our books indexed in the Book Citation Index
in Web of Science™ Core Collection (BKCI)

Interested in publishing with us?
Contact book.department@intechopen.com

Numbers displayed above are based on latest data collected.
For more information visit www.intechopen.com

Hybrid Silicon Nanowires: From Basic Research to Applied Nanotechnology

Muhammad Y. Bashouti, Matthias Pietsch,
Kasra Sardashti, Gerald Brönstrup,
Sebastian W. Schmitt, Sanjay K. Srivastava,
Jürgen Ristein, Jordi Arbiol, Hossam Haick and
Silke Christiansen

Additional information is available at the end of the chapter

1. Introduction

Silicon nanowires (SiNWs) have attracted particular attention in nanotechnology applications due to their unique advantages with respect to electrical, optical and thermoelectric properties compared to the planar thin films [1-3]. SiNWs show strong absorption of visible light in thin layers, which makes them attractive for the use in novel thin film concepts as in photovoltaics [4]. Like all the one-dimensional (1D) nanostructures, SiNWs have a large surface to volume ratio and thus surface-dominated properties that can be tuned, e.g. by suitable surface functionalization to be applied in sensitive sensors [5, 6]. Surface functionalization affects the overall electrical properties of SiNWs as dopants surface concentration, surface recombination rate, density of surface states, etc.[2, 7-10]. Atop Silicon atoms on SiNW surfaces can be terminated with a wide variety of molecules bearing covalent interfacial bonds i.e. Si-C [2, 7-10], Si-N [11] and Si-O [12]. Up to now we essentially exploited the Si-C bonds that permit a thorough control of the SiNW surface yielding a strongly reduced tendency to the undesirable oxidation of the SiNWs [2]. With such surface functionalization methods at hand, control and prediction of the electrical transport properties have become so viable that functionalized SiNWs can be considered as auspicious nanoscale building blocks in future high-performance nano-devices in the areas of electronics, opto-electronics, photovoltaics and sensing [13-18]. In this chapter we present a chemically-based surface functionalization method

based on Si-C bond surface termination that permits to fine-tune the electrical proper-
ties of VLS-grown SiNWs [2, 7-10, 19].

To date, electrical properties of SiNWs were controlled by doping with either boron (p-type)
or phosphorus (n-type) [20]. Electrical transport measurements indicate a reduced resistivity
according to higher doping levels and a tunable conductivity of doped SiNWs depending on
the gate potential (V_g) applied. Although changes of V_g provide temporary control of SiNW
conductivity, a more permanent and robust method is desirable for SiNWs to be useful in
nanoelectronic device applications.

A promising approach to control the electronic properties of SiNWs is to use hybrid mono-
layers (either polar or nonpolar molecules) that affects the surface state density and displays
an electrical potential on the surface/interface which modify the work function, electron af-
finity, surface Fermi level, and band offset/band bending at an interface [21-23]. This func-
tionalization effect is a general one and can be obtained with non-molecular treatments as
well [24]. Nevertheless, the use of molecules, especially organic ones, allows a systematic
tuning of the desired dipole moment by an appropriate choice of their functional groups
[25] or the intermolecular interactions between self-assembled molecules [10]. A surface
functionalization of SiNWs with organic functionalities can be as important as the effect of
the diameter and the wire orientation. In fact, due to the very high surface-to-volume ratio,
the functionalization of the surface and the immediate surroundings of the wire is expected
to have a dominant impact on its properties. Some computational studies have shown the
importance of passiveness in SiNWs [26, 27]. Similarly, the large surface-to-volume ratio in
SiNWs can be exploited in SiNW functionalization and used to modify transport properties.
SiNWs tend to form a layer of SiO_2 with thickness 1–2nm under ambient conditions. Subse-
quent HF treatment can be used to remove this oxide layer. Different Si surface treatments
can be performed to passivate SiNW surfaces with organic functionalities and obtain de-
sired electrical surface properties [2, 7-9].

2. Definition: What hybrid material means?

Although the term "hybrid material" is used to describe many diverse systems straddling a
widespread area of different materials, we restrict it by defining the concept as a composi-
tion and structure with/without interactions between the inorganic and organic units. In
general we can distinguish between two possible classes. *Class I* hybrid materials are those
that show weak interactions between the two phases, such as van der Waals, hydrogen
bonding or weak electrostatic interactions. *Class II* hybrid materials are those that show
strong chemical interactions between the components as in is our case.

2.1. Artificial strategies towards hybrid materials

There are two main approaches which are used to form hybrid materials:

1. Building block approach: A well-defined preformed matrix is applied to react with build-
    ing blocks to form the final hybrid material. Regularly, the matrix consists of at least one

functional group that allows an interaction with the building blocks. A representative example of this approach is the bonding of organic molecules to silicon surfaces.

2. In situ formation of the components: One or more structural units are formed from the precursors that are transformed into a novel network structure. In these cases well-defined discrete molecules are transformed to multidimensional structures, which often show totally different properties from the original precursors. Typical examples of this approach are polymer reactions and Sol-Gel techniques.

We use the building block approach since it has a main advantage associated with the *in situ* formation in which the structural unit will remain well-defined and usually does not suffer from significant structural changes during the hybrid-matrix formation. Additionally, the building blocks or the matrix can be designed independently in such a way to give the best performance and to be designed to our desire. For example polar or non-polar molecules can be attached to the silicon matrix for sensing application or for FETs applications.

2.2. Chlorination/Alkylation process

The organic building blocks were connected to SiNW surfaces following the building-block approach. We report on the functionalization of SiNWs with alkyl chains using a versatile two step chlorination/alkylation process [8]. The two step process found to be gentle in the sense that it did not break the matrix (i.e.) SiNWs or change their diameters.

The SiNWs were terminated with alkyl chains using a two-step chlorination/alkylation route (see Figure 1). Before any chemical treatment, each sample was cleaned by N_2 flow. After being cleaned, H-terminated SiNWs were prepared by etching the amorphous SiO_x coating by exposing the SiNWs to buffered HF solution (pH=5) for 60 s and then NH_4F for 30 s. The samples were then rinsed in water for <10 s to limit oxidation, dried in flowing $N_2(g)$ for 10 s, and immersed into a saturated solution of PCl_5 in C_6H_5Cl (0.65 M) that contained a few grains of $C_6H_5OOC_6H_5$ that act as a radical initiator. The reaction solution was heated to 90-100 °C for 5-7 min. Then the sample was removed from the reaction solution and rinsed in tetrahydrofuran (THF) followed by rinsing in methanol and then dried under a stream of $N_2(g)$. The Chlorine (Cl) terminated SiNWs were alkylated by immersion in 0.5 M alkyl Grignard, R-MgCl, in THF, with R= methyl (CH_3; hereinafter C1), ethyl (CH_3CH_2; hereinafter C2), propyl ($CH_3(CH_2)_2$; hereinafter C3), butyl ($CH_3(CH_2)_3$; hereinafter C4), pentyl ($CH_3(CH_2)_4$; hereinafter C5), or hexyl ($CH_3(CH_2)_5$; hereinafter C6), or Octyl($CH_3(CH_2)_7$; hereinafter C8), or Nonyl($CH_3(CH_2)_8$; hereinafter C9), or Decyl($CH_3(CH_2)_7$; hereinafter C10).

The reaction was performed for 5 to 4320 min (72 h) at 80 °C. At the end of the reaction time, the samples were removed from the reaction solution, rinsed in THF and methanol, and dried under a stream of $N_2(g)$. 2D Si (100) surfaces were alkylated following the procedure mentioned above, but with two minor differences:

i.   the samples were chlorinated (i.e., immersed in the hot solution of PCl_5) for 60 min

ii.   the alkylation time for all samples was 24 h.

These conditions were found to give the maximal coverage of alkyl chain on 2D Si(100). Alkylation of 2D Si(100) for 48 and 72 h gave similar coverage to those processed for 24 h.
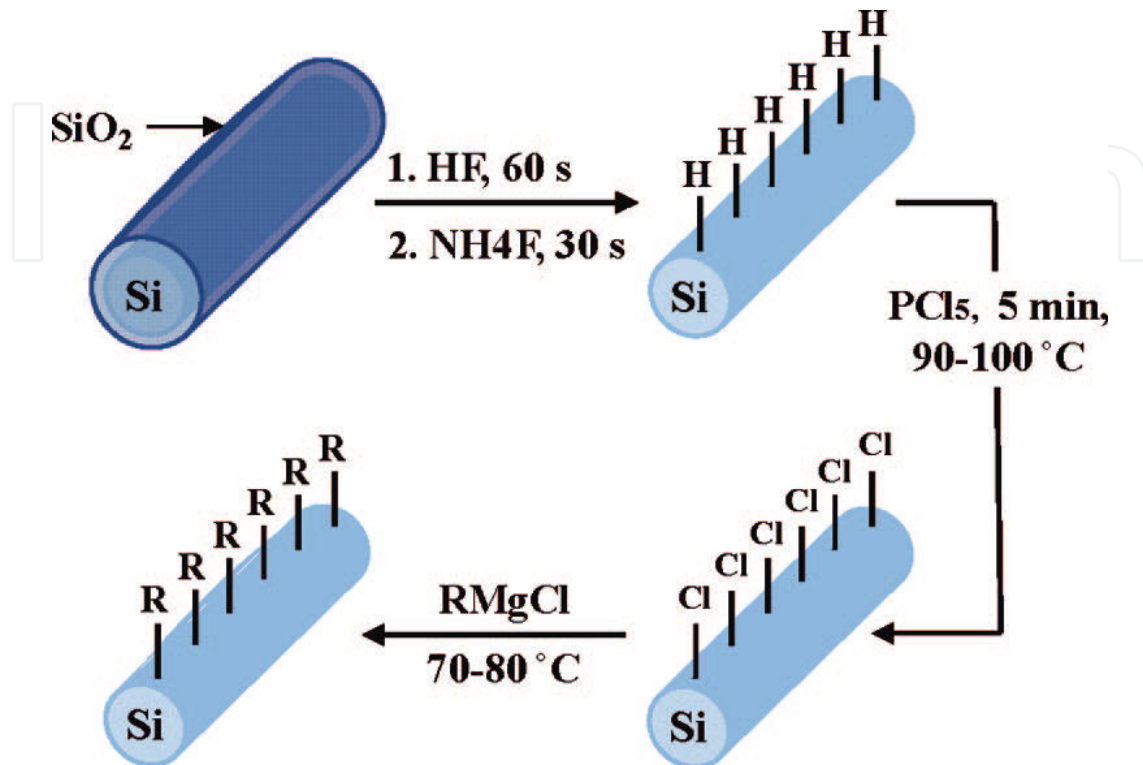

Figure 1. Scheme for illustrating the functionalization of SiNWs through the two step chlorination/alkylation process.

3. Fabrication of silicon nanowires

The SiNWs discussed in this chapter are grown by the well-known vapor-liquid-solid (VLS) mechanisms and a short description of the SiNWs growth will be given [28]. Si and Au form an eutectic that melts at 363°C while they individually melt at temperatures well above 1000°C. To grow SiNWs small gold droplets are dispensed on a Si wafer and inserted in a chemical vapor deposition (CVD) chamber. Then the samples heated up to 500°C i.e. above the eutectic temperature and below the melting points of each element. Si is supplied in vapor phase using silane (SiH_4) as the precursor. Si atoms enter the Au droplets causing their supersaturation of Si and the subsequent deposition of excess Si at the droplet-substrate interface. The VLS growth mechanism has its name due to the different states of the Si during the process. Different doping of the SiNWs can be obtained by introducing doping gases during the growth. Additionally, by the right choice of nanoparticle size, SiNWs diameters ranging from a few hundred nanometers down to a few nanometers can be obtained. The parameters of the CVD processes that are used for the SiNWs discussed in this paper are: growth pressure of 0.5 to 2.0 mbar, heater temperature of between 600°C and 700°C (since the heater was not in direct contact with the sample later temperature was considerably low-

er) and silane flow rate of 5 sccm using 5 to 10 sccm Ar as carrier gas. The grown SiNWs exhibit random orientation and usually gold nanoparticles on their tips (Figure 2).
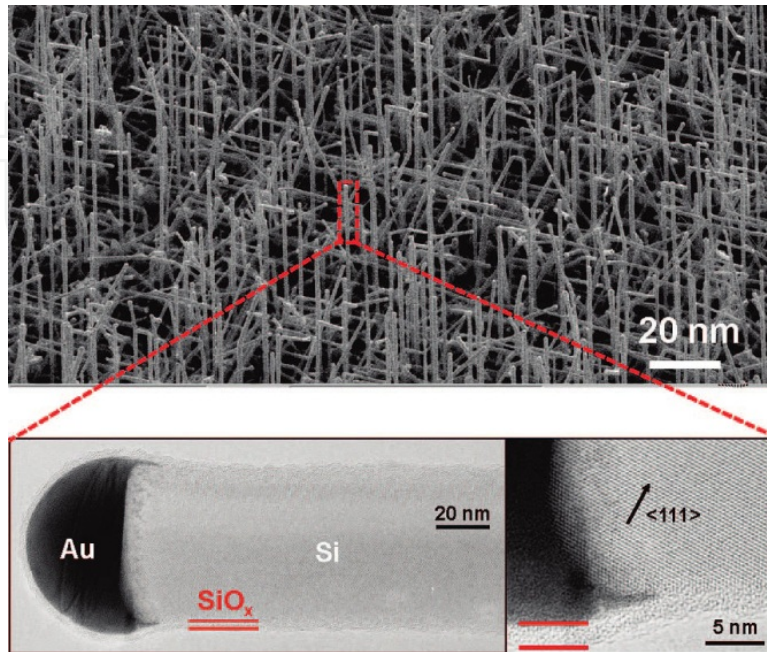

Figure 2. SEM image of SiNWs prepared by CVD on Si(111) substrates (upper part) and TEM images of an individual SiNW (lower part). The images indicate that the studied SiNWs consists of a 50±10 nm diameter Si core coated with 1-2nm of native SiO_x shell.

The Au nanoparticle from the catalyst is very mobile and diffuses over the SiNW surface (and inside the bulk regime).
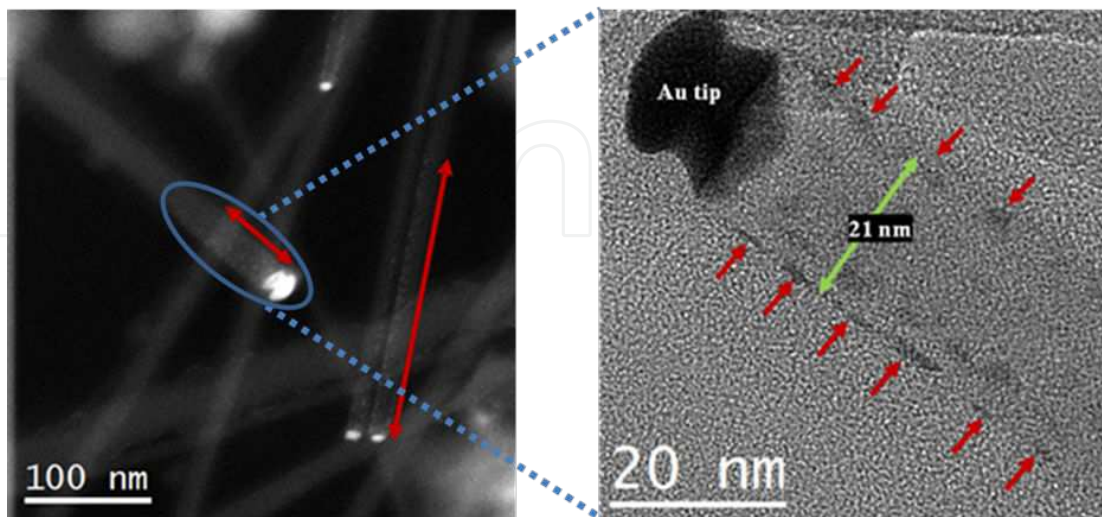

Figure 3. (a) HAADF-STEM general view of SiNWs, the red lines show the Au nanocluster extension. (b) HRTEM details of the selected area in Figure 3a.

This effect is enhanced in thin NWs and it was found from our previous report that Au nanoparticles can accelerate the oxidation on SiNWs [29]. 25-nm SiNWs show Au in the NW (in brighter contrast in Fig 3). Notice that Au is not only localized on the catalyst tip, but extends up to 300 nm apart from the tip. Figure 3a correspond to the HAADF-STEM general view of the NWs, the red lines show the Au nanocluster extension. Fig 3b corresponds to HRTEM details of the marked area in Fig 3a. In this case we have clearly observed that the presence of Au clusters (darker contrast), enhances oxidation rate in the thinner NWs relative to the thicker ones.

4. Molecular functionalization of CVD-SiNWs

Before any chemical treatment, SiNWs show a native oxide as illustrated previously in Figure 2. The oxide layer can be detected by X-ray photoemission spectroscopy (XPS) of the oxide core level spectrum. The Si2p of the oxide peak appears in the 101-104 eV binding energy range. In order to attach molecules to the SiNW surface, the native oxide has to be removed. This can be done by shortly immersing the SiNWs in HF and NH_4F solution. The XPS survey of the as-prepared H-SiNWs proved the thorough removal of oxides by the absence of any peak in the 101-104 eV as can be clearly seen in Figure 4.
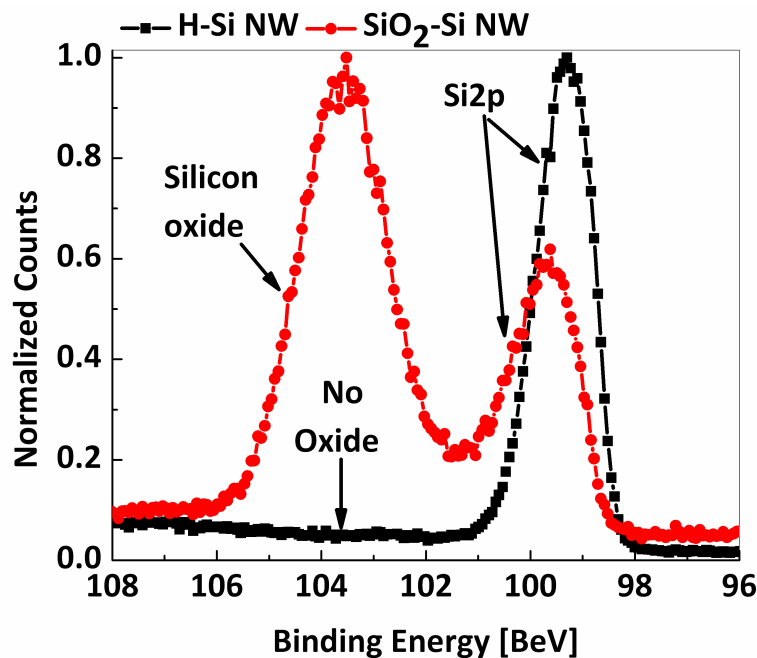

Figure 4. Si_2p emission of SiO_2-SiNW and H-SiNW.

It should be noted that the Si2p emission of SiO_2-SiNW is shifted towards higher binding energy as will be explained in the solar cell section. The emission of the C1s regime before and after termination is also compared in order to follow the covalent attachment of the molecules on the surfaces. Comparing the two emissions, an additional peak has to be introduced for molecule-

terminated SiNW surfaces to obtain an appropriate deconvolution (figure 5). Figure 5 depicts the XPS spectrum of C1s emission region for the hydrogen- and alkyl-terminated SiNWs. H-SiNWs' spectrum was fitted to two C-C at 285.20±0.02 eV, and C-O at 286.69±0.02 eV while the alkyl-SiNW was fitted to three peaks: C-Si at 284.11±0.02 eV, C-C at 285.20±0.02 eV, and C-O at 286.69±0.02 eV. The new peak at C-Si at 284.11±0.02 eV confirm the chemical bonding of organic molecules onto the SiNW surface. Peaks were typically adjusted to produce fits that minimized the difference between the full widths at half-maximum (fwhm).The center-to-center distances were fixed at 1.10±0.10 eV between the C-Si and the C-C emissions and at 2.60±0.10 eV between the C-O and the C-Si emissions. To attain the molecular coverage of surface atomic sites, the area under the C-Si peak is divided by the one under the Si2p peak (sum of $Si2p_{1/2}$ and $Si2p_{3/2}$) and normalized by the scan time. The coverage of the alkyl functionalities was compared with the highest value obtained for methyl (C1) functionality; in this instance "highest" means nearly full coverage of the Si atop sites, achieved after alkylation times of >24 h. This comparison is expressed throughout the text as "$(C\text{-}Si/Si2p)_{alkyl}/(C\text{-}Si/Si2p)_{max.methyl}$". Occasionally, a small signal due to oxygen was observed at 532.02±0.02 eV (O1s) and assigned to adventitious adsorbed hydrocarbons having oxygen bonded to carbon (286.69±0.02 eV) as shown before and after alkyl treatment. It is reasonable to assume that these adventitious hydrocarbons could stem from the wet chemical processing with THF solvent, THF/methanol rinse after functionalization, and/or carbonaceous materials present in the laboratory environment.
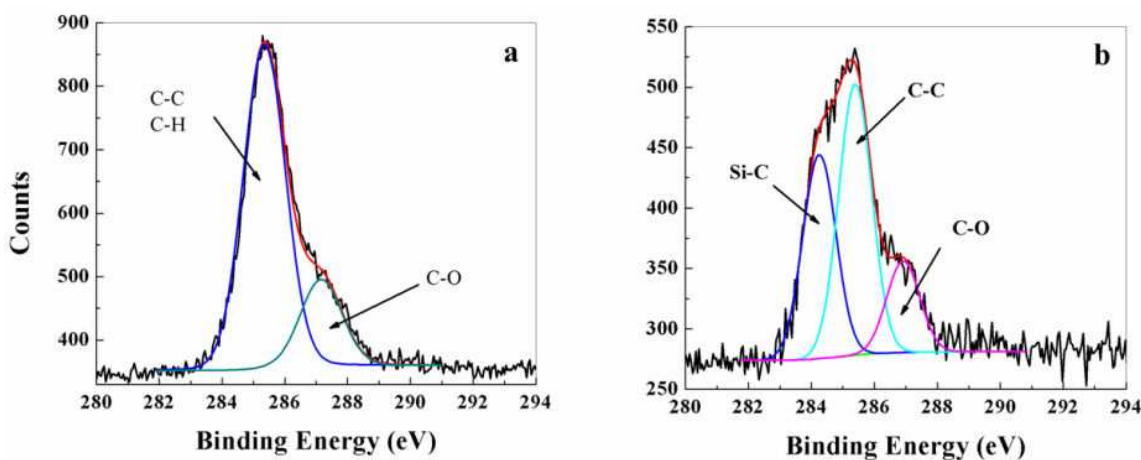

Figure 5. XPS data from the C1s emission region of the hydrogen and alkyl-terminated SiNWs. (a) H-SiNWs show two peaks: C-C at 285.20±0.02 eV, and C-O at 286.69±0.02 eV. (b) Alky-SiNWs, show three peaks: C-Si at 284.11±0.02 eV, C-C at 285.20±0.02 eV, and C-O at 286.69±0.02 eV.

The absence of SiO_x signal in the Si2p spectral surveys supports the argument that the O1s signal arises from physical bonding of hydrocarbons. Moreover, lack of F1s signal (which appears at 686.01±0.02 eV binding energy), confirmed that the $NH_4F_{(aq)}$-etched Si surface was not terminated by Si-F species.

Figure 6 shows the "$(C\text{-}Si/Si2p)_{alkyl}/(C\text{-}Si/Si2p)_{max.methyl}$" ratio as a function of alkylation time. As shown in the figure, the longer molecular chain requires a longer time for alkylation. For example, the time required to achieve 92±3 % of the saturation level in the adsorption curve,

Γ_{sat}, for C1 functionality, stands at 20±2 min. Increasing the chain length to C6 increases Γ_{sat} to 120±10 min, while the maximum coverage that could be achieved is merely 56±10 % of C1-SiNWs. Longer alkylation times, up to 24 h, changed the total coverage by 5±3 %. Alkylation times of 24 to 72 hours did not further change the coverage on SiNWs and planar Si(100).

Table 1 summarizes the Γ_{sat} values for many of the molecules presented in our former studies, along with the related $(C\text{-}Si/Si2p)_{alkyl}/(C\text{-}Si/Si2p)_{max.methyl}$ ratios. As observed in the table, C2-SiNWs show a "$(C\text{-}Si/Si2p)_{ethyl}/(C\text{-}Si/Si2p)_{max.methyl}$" value of 68±3 %, indicating that C2 groups can be packed at a relatively high density without major steric effects. C3, C4, C5, C6, C8 and C10 produced 56±5 %, 49±5 %, 50±10 %, 56±10 %, 56 ±10 %, and 80±10 % coverage, respectively, much higher than those of the same molecules on 2D Si (100) substrates (30±20 %,). Furthermore, the time required to achieve maximum coverage of the molecules on SiNWs is 4-30 times shorter than that of the 2D substrates. Using simple geometrical considerations, the gain in the steric hindrance on surfaces of 50±10 nm (in diameter) SiNWs is marginal. This cannot explain the higher molecular coverage on SiNWs, compared to 2D Si(100). Indeed, gain in steric hindrance between the adsorbed organic molecules starts to be important in NWs with <10-20 nm in diameter. This conclusion claims that the observed differences in coverage are related to different kinetics and higher available reactive sites on SiNWs, compared to 2D Si(100). The observation of 0.11±0.02 eV higher binding energy for a specific alkyl-terminated SiNWs, compared with equivalent 2D Si(100) surfaces, could further support the higher reactivity of SiNW atop sites. The broadening of Si2p fwhm in the SiNWs case suggests, compared to 2D Si(100), that wider distribution of bond strengths exist on the surface, thus leading to a wider distribution of reactive sites [30].
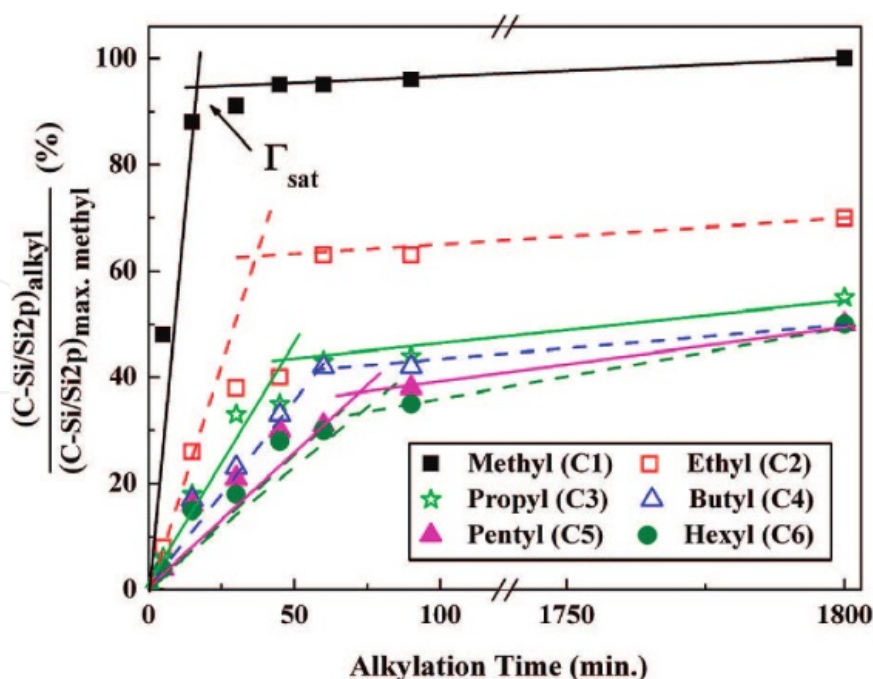

Figure 6. Coverage of alkyl molecules of SiNW atop sites as a function of alkylation time. Γ_{sat} stands for the time required to achieve92± 3 % of the saturation level of the adsorption curve.

| Alkyl molecule | Γ_{sat}(min) | Silicon Nanowire (SiNW) | | | 2D Si(100) |
		C-Si/Si2p	Max. Coverage		Max. Coverage
C1	20±2	0.135±0.001	100±5%		100±5%
C2	50±10	0.093±0.002	68±5%		60±20%
C3	60±10	0.075±0.003	56±5%		30±20%
C4	65±10	0.066±0.004	49±5%		30±20%
C5	90±10	0.068±0.005	50±5%		30±20%
C6	120±10	0.076±0.006	56±5%		30±20%
C8	"/>120	0.075±0.007	56±5%		30±20%
C10	"/>120	0.108±0.009	80±5%		30±20%

Table 1. Summary of the XPS results for C1-C6 alkyl chains bonded to SiNWs and 2D Si(100) surfaces via Si-C bond

4.1. Early stages of oxide growth in H-SiNWs

To examine the thermal stability of H-SiNWs, the native oxide shell on SiNWs was etched away by hydrofluoric acid and ammonium fluoride. Subsequently, freshly etched SiNWs were annealed in ambient conditions (with average humidity of 30 %) in seven distinct temperatures of 50 °C, 75 °C, 150 °C, 200 °C, 300 °C, 400 °C and 500 °C, each for five different time-spans: 5 min, 10 min, 20 min, 30 min and 60 min. After each heating stage, the specimens were examined by XPS. To identify various sub-oxide states in the Si2p spectrum, spectral decomposition was performed by a curve-fitting procedure, using Gaussian-Lorentzian functions after a Shirley background subtraction as shown as example in Figure 7. The sub-oxides states and their respective chemical shifts (Δ) relative to the $Si2p_{3/2}$ (at 99.60± 0.02 eV) are as follows: $Si2p_{1/2}$ (Δ=0.60 eV), Si_2O (Δ=0.97 eV), SiO (Δ=1.77 eV), Si_2O_3 (Δ=2.50 eV), and SiO_2 (Δ=3.87 eV). The shift in binding energy is dependent on temperature and time (dashed line in Figure 7a). Generally speaking, upon the formation of sub-oxides and SiO_2, the Si2p peak moves to higher binding energies to compensate the band bending and surface Fermi level shift as the oxide layer grows (not shown). The intensity of a sub-oxide (I_{ox}) is expressed by the ratio of the integrated area under its peak to the Si2p peaks overall area ($Si2p_{3/2}$+$Si2p_{1/2}$) i.e. the total intensity of unoxidized silicon atoms. Sub-oxide intensity can be expressed in terms of the number of monolayers formed corresponding to the intensity of 0.21 per monolayer [31].

Figure 8 depicts the variation of the average number of monolayers over time for individual sub-oxides (I_{ox}) and the overall oxide intensity ($I_{tot}=I_{Si2O}$+ I_{SiO}+I_{Si2O3}+I_{SiO2}) for low-temperature (T < 200 °C, Figure 8a) and high-temperature (T ≥200 °C, Figure 8b) oxidation of H-SiNWs. Comparison of the sub-oxides growth in Figure 8 illustrates their temperature and time dependence. In both temperature ranges, Si_2O is present even in the etched surfaces with intensity of I_{ox}=0.02±0.01 i.e. ~0.2 monolayer and its intensity plateaus at the value of I_{ox}=0.06±0.01 (~0.25 to 0.3 monolayer) at the very early stages exhibiting negligible growth over the whole time range. SiO and Si_2O_3 exhibit approximately identical behavior and values in both ranges despite the plateau region occurs 15 minutes earlier in the high tempera-

ture range. They exhibit no peak at t=0 and an intensity of 30-60 % of the maximum intensity after 5 min and 20 min for high and low temperature regime, respectively. However, at T ≥ 200 ˚C, SiO and Si_2O_3 have 0.2 monolayer coverage that is twice as large as coverage in T < 200 ˚C (~0.1 monolayer). The behavior of the transient sub-oxides versus oxidation time is similar to that of SiNWs exposed to molecular oxygen wherein the intensities of the transient sub-oxide almost remain constantly below one monolayer. Conversely, SiO_2 intensity was found to strongly rely on the temperature and time and two regimes of fast and slow growth were clearly recognized.
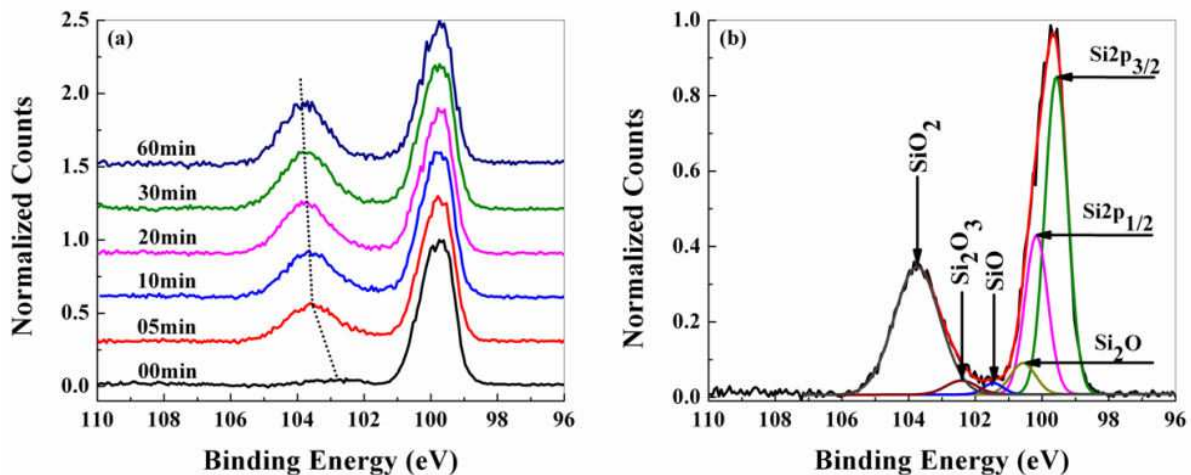

Figure 7. (a) An example of Si2p XPS spectra of the H-SiNW surfaces annealed at 500 ºC for different times; the inclined dashed line represents the blue shift upon formation of the oxide layer. (b) Decomposed Si2p sample spectrum of oxidized SiNWs illustrating four different suboxides including Si_2O, SiO, Si_2O_3 plus the stoichiomertic SiO_2 at 100.6 eV, 101.7 eV 102.5 eV and 103.4 eV, respectively.
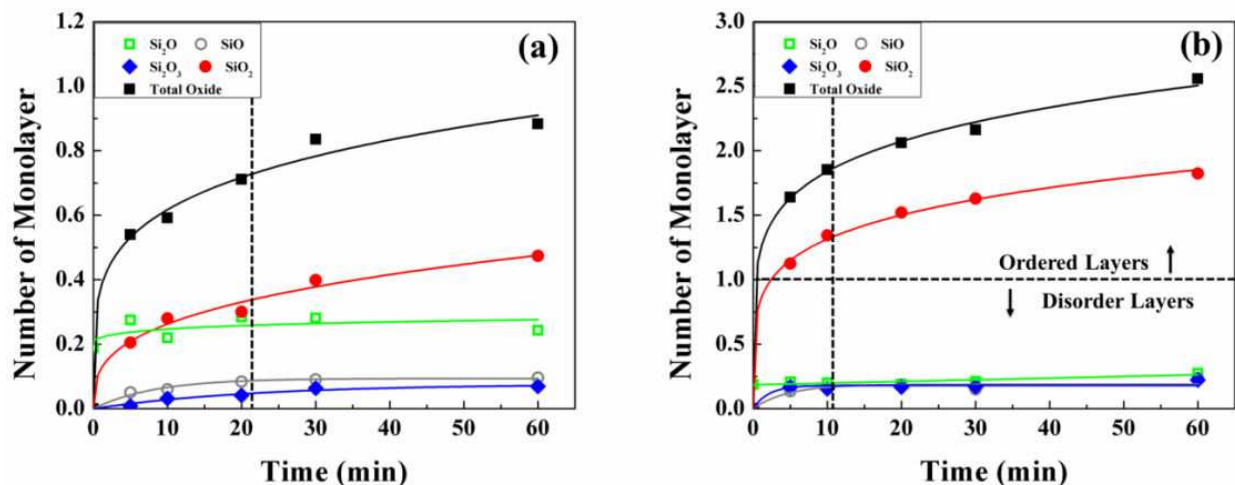

Figure 8. Number of monolayers over time for the sub-oxides Si_2O (green), SiO (gray), Si_2O_3 (blue), SiO_2 (red) and their sum as total oxide (black) in the two low-temperature (a) and high-temperature (b) regimes. The vertical dashed lines represent Γ_{sat}, while the horizontal one in (b) defines the onset for ordered oxide layer formation.

At higher temperatures (T≥200 °C), the time required to achieve 70±10 % of the final intensity (defined as Γ_{sat}) for SiO_2 is 10±2min, while at lower temperatures (T<200 °C), Γ_{sat} shifts to 18±2min. On the other hand, Γ_{sat} for the total oxide amount lies approximately on the same times as SiO_2 demonstrating its sizable weight in the total oxide amount. Therefore, temperature dependence of oxide growth can be well observed in Figure 9a that depicts the total oxide vs. time for all tested temperatures. According to the TEM measurements the extension of the annealing period at 500 °C from 1 hour to 24 hours results in an increase of oxide layer thickness from 4.5nm to 6nm. Thus, 23 hours of further annealing leads to less than 35 % increase in oxide thickness that is noticeably smaller than the growth observed at the starting times and the graph after Γ_{sat} can be assumed as a plateau like sub-oxides plots.

Early stages of high temperature oxidation in H-SiNWs can be modeled by the modified Deal-Grove model taking into account partly or completely sub-oxides as growth sites with varying concentrations over time and temperature [32, 33]. Nonetheless, above Γ_{sat} a linear Deal-Grove regime cannot be accommodated with the approximately flat tail of the SiO_2 plot and a limiting mechanism is required to interpret such a behavior [34]. Between Γ_{sat} and maximum oxidation (1 hour) at high temperatures, a significant fraction of the superficial Si atoms are surrounded by fourfold occupied oxygen sites with high local strains that act as a barrier for further oxidation. Under this conditions, oxidation hindrance can be caused by two phenomena: self-limiting oxide film formation (seen in 2D Si) [32] and self-retarding oxidation known for SiNWs and their particular geometry [35]. However, self-retarded oxidation becomes more significant on curved surfaces like SiNWs at diameters below 35 to 44 nm due to the extremely small amount of viscous flow in the oxide layer that could relax the applied stresses [36]. On the other hand, repetition of the same measurements for Si2D resulted in the same flat end for the I_{ox}-t plot at T ≥ 200 °C (Figure 9a and 9b). Therefore, the inhibited oxide growth in the high temperature region is better understood as a result of self-limited oxidation rather than geometrical compressive that can be neglected for the current NWs. Non-retarded growth of oxide at 500 °C (Figure 9a) can be associated with partial melting at NW surfaces causing accelerated oxygen diffusion and NWs fragmentation (6 times length decrease) which led to deeper oxygen penetration and larger interfacial areas (Figure 9b and c).

At low temperatures Γ_{sat} of SiO_2 is shifted to longer times (18±2min) and transient sub-oxides are the main sources for the total oxide intensity at times between 0 and Γ_{sat} (Figure 8b). Based on our earlier work, heating above 450 °C can remove all the Si-H bonds on flat Si wafers [37]. At lower temperatures and initial times (i.e. before <Γ_{sat}), the oxidation occurs in the presence of functionalizing H atoms and OH groups (resulted from water vapor interaction with the surfaces). Therefore, oxidation proceeds thorough Si-Si backbond oxidation forming sequentially peroxidic and disiloxanic bonds in the first few atomic layers. Nevertheless, heating in the atmosphere of 30 % average humidity, water assistance to early oxide growth and corresponding oxidation-hydroxylation cannot be neglected [38, 39]. To understand the relation between the rate-determining step and the surface bonds strength, we studied methyl-termination of

SiNWs, which naturally provides the same coverage as hydrogen functionalities but with Si-C bonds, instead [19, 30]. Interestingly, when exposed to air at room temperature for 44 days, SiO_2 formation was relatively suppressed, while Si_2O intensity was equal to the one for H-SiNW [8, 40]. After the 44-day period, methyl-terminated SiNWs showed I_{SiO_2} intensity of 0.11; it almost equals that of H-SiNWs after 1 hour. This can be explained by the lower susceptibility of Si-Si underlying bonds in Si-C covered surfaces compared to Si-H covered ones [30]. For further oxidation at lower temperatures however, the electron or hole tunneling mechanism proposed for Si(100) room temperature oxidation encounters difficulties to be proven considering the fact that neither individual sub-oxides nor total oxide amount reaches the level of a single monolayer [41]. Alternatively, rupture of the surface bonds may act as the second oxidation source after local development of the backbond Si-O. In this respect, in methyl-terminated SiNWs monotonic growth of sub-oxides and SiO_2 has been observed after a dramatic decline in the amount of Si-C concentration. Similarly, bond propagation can be conceived in H-SiNWs with a relatively lower resistance to the oxidizing species [30].

Figure 9d shows the temperature dependence of the total oxide formation rate in the 2D Si and H-SiNWs specimens before Γ_{sat} for all the temperatures investigated in this study. High and low temperature data points are fitted in two different lines for each specimen. Near-linear behavior of oxidation rate logarithm vs. reciprocal of temperature at the early stages of oxidation allows us to calculate respective activation energies (E_A^{ox}) based on the Arrhenius equation. In the high temperature region 2D Si and SiNWs exhibit E_A^{ox} of 46.35 m eV and 48.22 m eV, respectively. Such a minor difference in the activation energy magnitudes denotes again that geometrically-induced stresses affect negligibly the rate-determining step. Large divergence from values of activation energies for the linear Deal-Grove model (1.83 to 2.0 eV) approves that the rate is rather determined by the growth sites development than by surface oxidation reaction. In addition to sub-oxide islands, near-interfacial remnant silicon atoms may contribute to the oxidation process as growth sites [33, 42]. Moreover, higher absolute intensities and oxidation rate values for SiNWs at 500 °C beyond the first 10 minutes compared to 2D Si necessitate the existence of a growth-site-enhancing mechanism as partial melting of SiNWs. This mechanism improves the oxygen permeability to deeper layers and increases the interfaces due to NW fragment formation (Figure 9c).

For the low temperature regime E_A^{ox} values of 35.20 m eV for 2D Si and 23.31 m eV for SiNWs were also calculated. Lower activation energies for SiNWs may correspond to the strain induced by dangling bonds rebonding at the (110) and (111) adjoining surfaces as well as higher ratio of ambient exposure area to the oxide/silicon interface area [43]. Stretching weakens the very first layers of silicon backbonds and results in their higher susceptibility to bond rupture and suboxide formation. Conversely, bending stresses are able to increase robustness of hydride terminations (di- and trihydrides) on the surface and lower the SiNW oxidation rate at higher temperatures where surface bond propagation determines the overall rate (for 75 °C and 150 °C where rates are lower than 2D Si).

All the above descriptions suggest the following mechanism (schematically shown in Figure 10): (i) At low temperatures, Si-Si backbond oxidation and later Si-H bond propagation are the rate-determining steps. (ii) At higher temperatures, the oxygen diffusion is considered as the rate-determining step initially through controlling the growth sites concentration (conserving some Si-H interfacial bonds) where disorder monolayer still dominates the oxide intensity. Beyond Γ_{sat}, the reaction shifts to almost zero-order which denotes a self-limiting process because initially formed oxide shells prevent a further oxidation. A fraction of the Si-H bonds converted to Si-OH according to H_2O molecules present in the surrounding atmosphere.
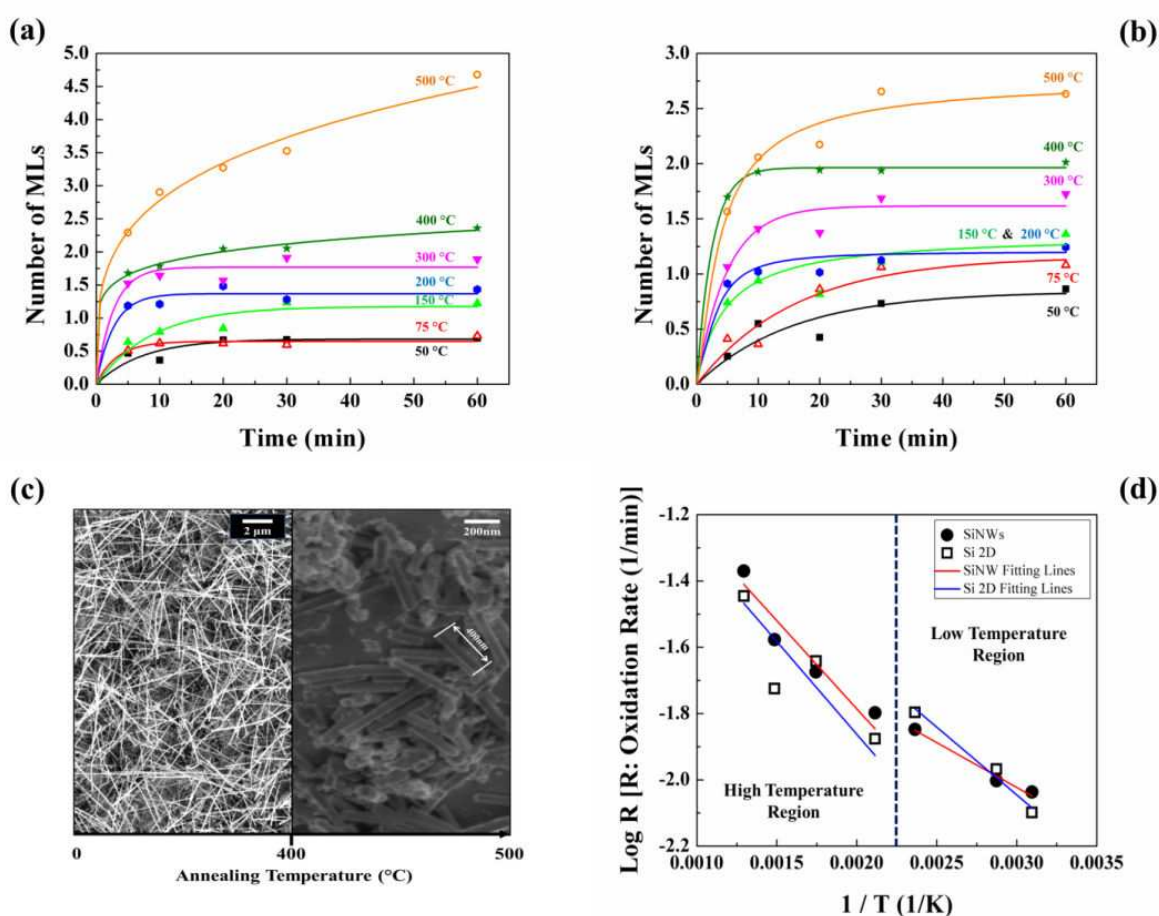

Figure 9. Oxide monolayer growth over time for H-SiNW surfaces (a) and 2D H-Si (b) oxidized at different temperatures for time spans ranging from 5 to 60 min. (c) Comparison between pristine (right) and melted (left) SiNWs. (d) Temperature dependence of oxide formation in H-SiNWs and 2D Si in air between 50°C and 500°C. For all temperatures, the annealing time is below Γ_{sat}.
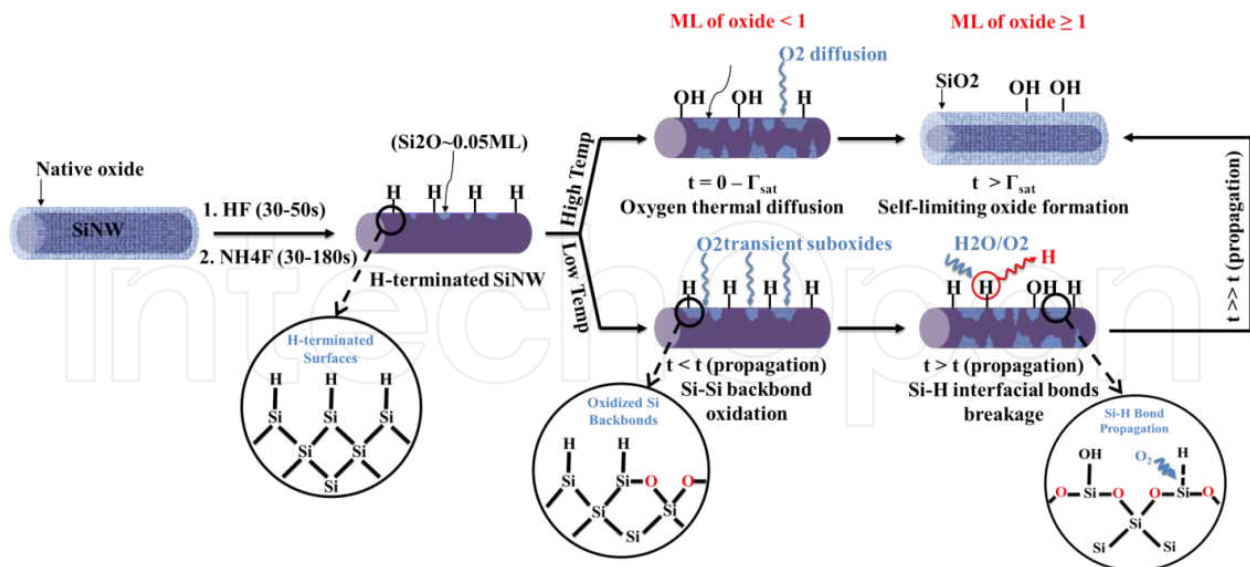
Figure 10. Schematic graph summarizing the inferred oxidation mechanism for H-SiNWs. The blue spots represent the sub-oxide islands. Interfaces at different stages of low-temperature oxidation as well as initial H-terminated one sare depicted in more detail in circles.

4.2. Stability of molecules on SiNWs in long time

To investigate the stability of the alkylated SiNWs, freshly prepared SiNWs having maximum coverage of alkyl functionalities (mostly obtained after alkylation time of 24 h) were exposed to ambient air for several hundreds of hours (Table 2). Oxide intensity in SiNWs functionalized by methyl and ethyl equals zero up to 48 hours. After 336 h of exposure, oxide intensity reached 0.03 (~0.14 monolayer) for C1-SiNWs and 0.05 (~0.23monolayer of oxide) for C2-SiNWs. In contrary, after 24 hours of exposure, oxide intensity in SiNWs terminated with C3 to C6 rose to 0.01 (~0.05 monolayer of oxide), 0.02 (~0.10 monolayer of oxide), 0.02 (~0.10 monolayer of oxide), and 0.01 (~0.05monolayer of oxide), respectively. This implies that SiNWs terminated with C3-C6 alkyl molecules exhibit less stability against oxidation compared to C1- and C2-SiNWs. Nevertheless, after 336 hours, oxide intensity of C3- to C6-terminated SiNWs have approximately the same magnitudes (~ 0.13). From the data in Tables 1 and 2, with a wider perspective, it can be deduced that the shorter the alkyl chain, the lower the $SiO_x/Si2p$ ratio and the less liable to oxidation the terminated SiNWs.

These observations can be explained by the fact that the shorter the molecular chains, the lower the coverage of the alkyl molecules and the higher the probability of interaction between oxidizing agents (O_2 and H_2O) and molecule-free sites (or pinholes).The oxidation degree of the SiNWs was compared to planar Si(100) surfaces alkylated with the same series of molecules. C1-SiNWs exposed to air over a period of 336 h illustrated ca.4-fold lower oxidation intensity than the equivalent Si(100) surfaces, despite alike initial coverage levels. Similarly, C2-SiNWs exhibited ca. 3-folds lower oxide intensity than C2-Si(100). In contrast, (C3-C6)-SiNWs oxide amount was comparable to those of planar (C3-C6)-Si(100) after 336 h. These observations could be attributed to stronger Si-C bond on SiNWs surfaces. This can be

supported by the shift in Si-C energy bond of C1 terminations from SiNW (284.22±0.02 eV) to planar Si(100) (284.11±0.02 eV). Stronger bonding of surface functionalities has also been observed in H-terminated SiNWs. Respective studies suggest that the robustness of the SiNW's surface hydride (or alkyls) is a consequence of bending stresses being developed at the edge of two adjoining facets of a SiNW.

| | exposure time to air | | | |
Sample	0 hr	24 hr	48 hr	336 h
C1-SiNW	0	0	0	0.03
2D C1-Si(100)	0			0.11
C2-SiNW	0	0	0	0.05
2D C2-Si(100)	0	0.03	0.08	0.13
C3-SiNW	0	0.01	0.07	0.13
2D C3-Si(100)	0			0.15
C4-SiNW	0	0.02	0.07	0.13
2D C4-Si(100)	0			0.15
C5-SiNW	0	0.02	0.06	0.14
2D C5-Si(100)	0			0.16
C6-SiNW	0	0.01	0.06	0.12
2D C6-Si(100)	0	0.04	0.08	0.18

Table 2. Summary of the Oxidation intensity (SiOx/Si2P Ratio) for Alkylated SiNWs and 2D Si(100) Surfaces, Having Maximum Coverage (Mostly, Obtained after 24 hrs of Alkylation Time), at Different Exposure Times to Ambient Air.

4.3. Stability of Si-C bond on SiNWs

SiNW surfaces were terminated by CH_3 and compared with equivalent planar CH_3–Si surfaces having same surface coverage with Si–C bonds. Figure 11 shows the coverage of methyl functionalities as a function of alkylation time. Comparing the alkylation kinetics on SiNWs with 2D Si(100) showed two main notable differences: (I) 92±3 % of the maximum coverage on 2D Si(100) was achieved after 1000±50 min alkylation; (II) the reaction kinetics on 2D Si(100) at short and long alkylation times are rather different than on SiNWs. These differences in the kinetic behavior could be attributed mainly to differences in the surface energy. The cohesive energy becomes higher upon decreasing the dimensions of a given structure. Based on earlier work it can be seen that 50±10 nm (in diameter) SiNW surfaces has higher cohesive energy (~4.4 eV) than 2D Si(100) surfaces (~3.4 eV)[30, 44]. Furthermore, the broadening of Si2p fwhms in the case of SiNWs (data not shown), as compared to 2D Si(100) and 2D Si(111), suggests that wider distribution of Si–C bond strengths and/or ligands angle variations exists on the surface. Fig. 12 depicts variation of the SiO_2 intensity and molecular coverage over exposure time for both NWs and planar specimens of silicon. Since determining surface coverage requires accounting for escape length of photoelectrons, an ''impartial'' indicator was required to examine the robustness of the data presented in Fig. 12. With this in mind, ToF-SIMS experiments, by which the methyl coverage is proportional to the $SiCH_3^+$

(or CH₃⁻) fragments, can be carried out. ToF-SIMS results showed similar concentrations (within 5 % experimental error) of characteristic fragments in both CH₃–SiNWs and 2D CH₃–Si(100) substrates, marking the reliability of the XPS data presented in Fig. 11 and 12.
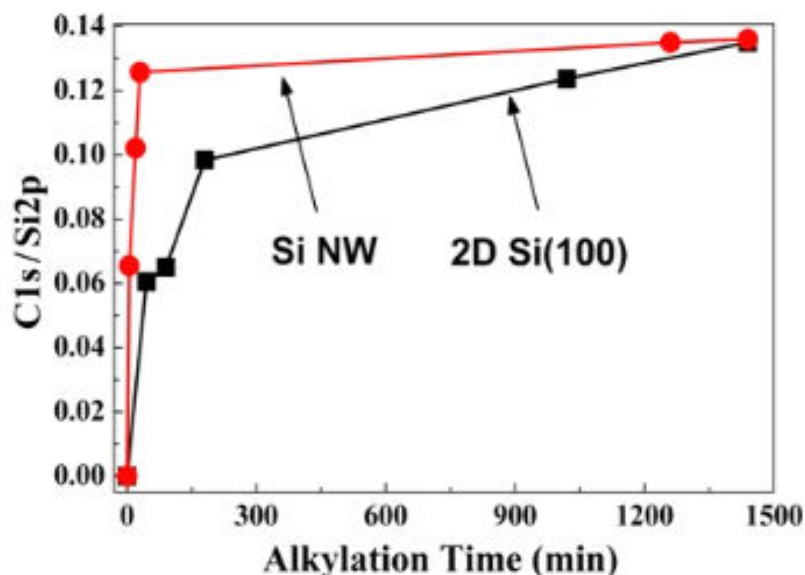

Figure 11. Coverage of methyl functionalities on 2D and SiNW as a function of alkylation time.

As shown in Fig. 12a, CH₃–SiNWs exposed to air over one month showed ca. 3-fold less oxidation than the equivalent 2D CH₃–Si(100) surfaces, albeit similar molecular coverage's in both structures. To attain a wider perspective, we made a comparison between 2D CH₃–Si(111) surfaces (naturally of 15–20 % coverage)and 2D CH₃–Si(100).
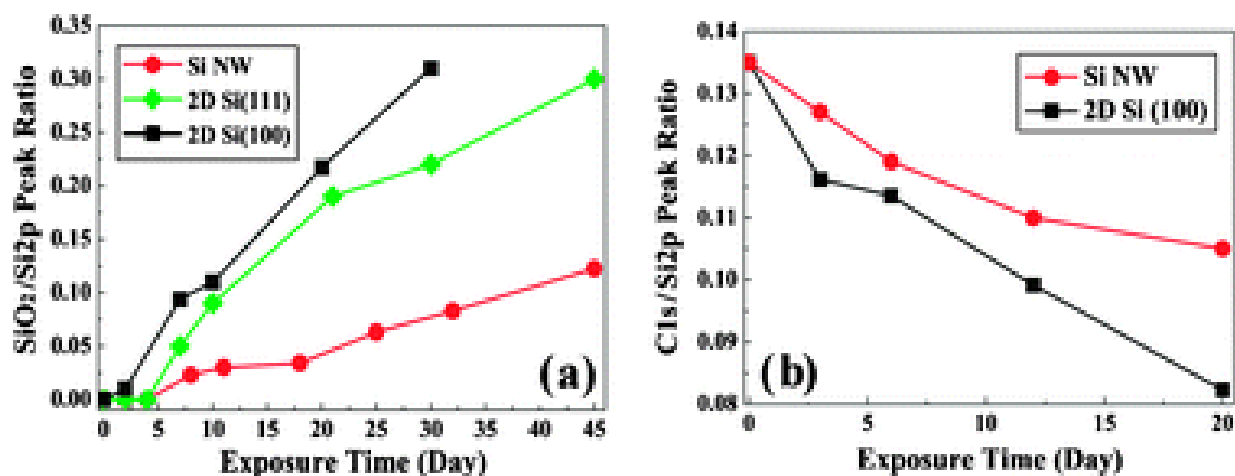

Figure 12. (a) Ratio of the oxidized Si2p peak area to the bulk Si2p peak area for the methyl modification of SiNWs, 2D Si(100), and 2D Si(111), exposed to air over extended time periods. (b) Si–C decay as a function of exposure time for SiNW and 2D Si(100). The measurements were done three times for each sample and averages have been taken.

Interestingly, in spite of notably lower coverage, 2D CH$_3$–Si(111) surfaces exhibit higher stability against oxidation than the equivalent 2D Si(100) surfaces, while they showed ca. 2-fold higher oxide intensity than the CH$_3$–SiNWs. This can also be referred to surface bond energy. The observation of ~0.11 ±0.02 eV higher binding energy for a CH$_3$–SiNW, compared to equivalent 2D CH$_3$–Si(100) surfaces, could further be ascribed to the higher reactivity of atop sites. Indeed, the CH$_3$–SiNW's C1s spectra showed 22 % decrease in the Si–C bond signal throughout 20 days, at the time which 2D CH$_3$–Si(100) specimen showed ~34 % decrease of the same signal (Fig. 12b). Surface bond strength dependency on structural geometry can be backed by the reports of Lee and co-workers on stronger H-termination of SiNWs relative to 2D Si surfaces suggested that the robustness of the SiNWs hydride is a consequence of bending stresses, where re-bonding of dangling bonds at the edge of two adjoining facets of a SiNW takes place [45].

Segment	Oxidation time CH$_3$-SiNWs		Oxidation time CH$_3$-SiNWs	
	0 days	4 days	0 days	4 days
Si-O	0.037±0.002	0.063±0.003	0.021±0.001	0.039±0.001
Si-C	0.142±0.006	0.091±0.009	0.074±0.001	0.039±0.001
Si-CH3	0.239±0.011	0.202±0.013	0.382±0.041	0.301±0.010
Si$_2$OC2H$_6$	0.004±0.001	0.008±0.001	0.004±0.0002	0.003±0.0002
SiO$_2$	0.071±0.002	0.139±0.002	0.030±0.0005	0.066±0.0003

Table 3. SiC$_x$H$_y$$^+$ peak intensities of ToF-SIMS spectra of SiNWs before and after 4 days exposure to an oxidizing atmosphere

To understand the relation between strength of the Si–C bond and the oxidation resistance, ToF-SIMS fragments of CH$_3$–SiNWs and 2D CH$_3$–Si(100) surfaces were collected after different exposure periods to the oxidizing agents. Table 3 presents the selected ToF-SIMS spectrum peak intensities of CH$_3$–SiNW before and after 4-day exposure to pure O$_2$(20 %)–N$_2$(80 %) environment of 10–15 % relative humidity (RH). After 4 days of oxidation, Si$_x$O signal (where x = 1,2) of SiNW samples increased by 70–95±10 % while the concentration of Si–C and Si–CH$_3$ bonds decreased by 36±2 % and 15± 2 %, respectively. Higher changes in the Si$_x$O signal suggest higher molecule-free Si–Si backbonds susceptibility to bond rupture upon interaction with oxidant molecules, than the Si–C bonds. And higher changes in the Si–C (36±2 %) signal than Si–CH$_3$(15±2 %) indicates that Si-Si bonds adjacent to the CH$_3$ groups are less prone to oxidation than Si-C surface bonds. Moreover, the results point out the early breakage of Si–Si back-bonds to form Si–O–Si back-bonds. After oxidation of the entire Si–Si back-bonds, oxidizing species start attacking the Si–C bonds. For 2D CH$_3$–Si(100) surfaces, the Si$_x$O signal increased by 86–120±10 % while the concentration of Si–C and Si–CH$_3$ bonds decreased by 47±2 % and 21±2 %, respectively, after 4 days of exposure to the oxidizing atmosphere. Evaluating the relative changes obtained for 2D CH$_3$–Si(100) surfaces and CH$_3$–SiNWs calls for two main conclusions: (1) CH$_3$–SiNWs are more stable than 2D CH$_3$–Si(100) surfaces, in consistency with the XPS observation, (2) The oxidation mechanism of 50±10 nm (in diameter) CH$_3$–SiNWs is similar to that of 2D CH$_3$–Si(100) surfaces.

4.4. Effect of chain length of alkyl molecules

According to theoretical simulations, steric effects (van der Waals diameter) can hinder for-mation of dense packing of alkyls longer than C1. Therefore, increasing length of the alkyl chains increases the van der Waals diameter from 2.5 Å (in the case of C1) to more than 4.5-5.0 Å for longer alkyl chains. The latter van der Waals diameters are much larger than the internulecular distance between adjacent Si atoms (3.8 Å), a matter that decreases their adsorption rate and limits their coverage to maximum 50-55 % of a monolayer of Si surface sites. With these findings in mind, we found the chain length dependence in Figure 13 to be consistent with the similar decay of the coverage reported by others on flat Si(111) surfaces for longer chains than in the present work, with, no increase of coverage above 7 carbon atoms [46]. Based on these inconsistencies it can be inferred that the higher coverage ob-tained for >C6 chain lengths is artificial and/or not significant owing to the problems in fit-ting of the XPS data. In contrast, few experimental observations suggest that the coverage behavior of chains longer than C6 on SiNWs might not be artificial, as justified by the fol-lowing explanations: (1) ToF SIMS experiments (which eliminate potential artificial observa-tions) have shown higher absolute coverage long chain lengths, in good consistency with XPS observations. (2) In the case of 2D Si(100) surface, the results of ToF-SIMS have shown (more or less) the expected coverage versus chain length behavior; at the time, similar be-havior was not observed in the case of SiNWs. (3) The experimental error and/or accuracy of the peak fitting are relatively small (4-11 %).
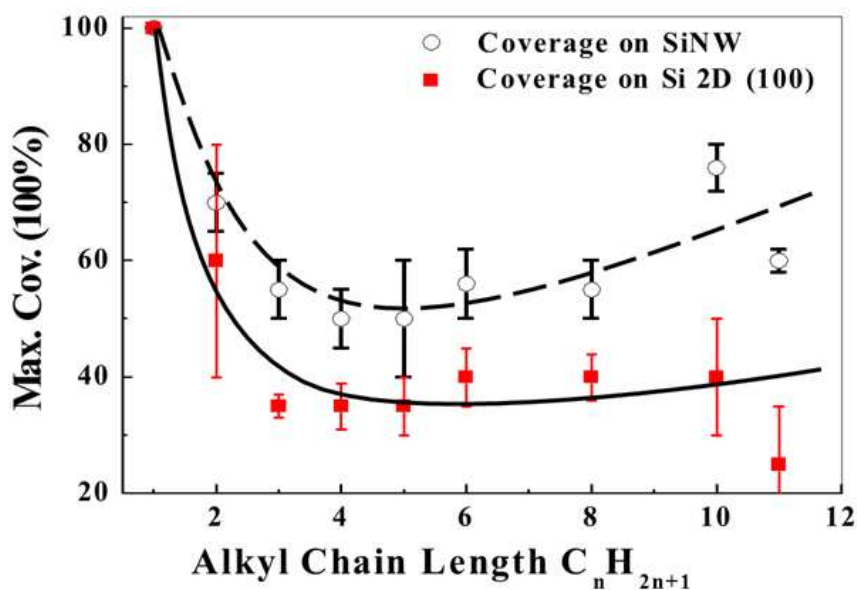

Figure 13. Max-alkyl versus alkyl chain length on SiNWs and, for comparison, on 2D Si(100) surfaces.

It is reasonable to consider passivation of SiNWs by alkyl molecules as a function of two main factors: (I) molecule-molecule lateral interaction and (II) molecule-substrate vertical in-teraction. For short alkyl chains (C1-C5), which exhibit liquid-like behavior and thermal fluctuations [47] the determining factor is the vertical interaction. Increasing the chain length

to C6-C10 forms a solid-like phase, where the lateral interactions become more dominant in the consequent coverage of the SiNW surfaces. It is worth pointing out that the lateral interactions between long alkyl chains might be formed during the physisorption stage, before the covalent bindings between the carbon and silicon atoms (or chemisorption) arise [48].

5. Integration of hybrid SiNWs into technological devices

Hybrid SiNWs modified by covalent Si-C bonds showed excellent atmospheric stability, high tansconductance values, low surface-defect densities, and allowing formation of technically-feasible air-stable SiNW field-effect transistors (FETs) and SiNW-photovoltaics [9, 19]. Here we demonstrate the electrical characteristics of such SiNW-based devices molecularly modified by the two-step chlorination/alkylation method. Analyses suggest that extrinsic effects (i.e. surface states and surface charge) accompanied by the adsorption of molecular layers significantly affect the FET and solar cell characteristics.

5.1. Fabrication of the FET

SiNWs were manufactured through a top-down approach based on electron beam lithography rather than the bottom-up VLS growth. It initiates from a bonded SOI wafer, with a thin (100 nm) top Si (100) layer (resistivity of 10–20 Ωcm) insulated from the (100) silicon substrate (resistivity of 0.8–1.2 Ωcm) by a silicon dioxide layer (380 nm). Surface was covered by a bilayer PMMA and mask definition was then performed by high-resolution e-beam lithography. The resist was then developed in a solution of MiBK:IPA (1:3). The pattern was transferred from the PMMA to the top SiO_2 layer by buffered HF etching. The central region, where the silicon was defined, was linked through small connections to the device leads. Subsequently, a 35 wt % KOH solution, saturated with isopropyl alcohol (IPA), was used to etch a single NW in the central region. Due to the anisotropy in etching, NW exhibits a trapezoidal cross-section. After this step, the aluminum contacts were defined by means of a lift-off process. The SiNWs, after the silicon etching, had a length (L) of 1mm, a top width (w) of 70 nm, a height (t) of 100 nm, and trapezoid base (W) (of 200 nm, as illustrated in figure 14. The diagonal is based on (111) planes, whereas atop side is made up of a (100) plane. The available starting material had a resistivity of 10–20 Ωcm. At the end of the fabrication process, the Al electrodes were coated with PMMA to protect them from etching agents (e.g., buffer HF, NH_4F, etc.) during the alkylation process. To assess the electrical characteristics of the various SiNW FETs, voltage-dependent back-gate measurements were performed in a probe station (Cascade Microtech Femtoguard, Summit/S300-11741B-6, USA) under the ambient conditions. In these measurements, back-gate voltages (V_g) of -20 V to +20 V, in steps of 1 V, were applied to the silicon substrate, of which the doping level is high enough such that the band bending in the Si substrate is negligible under operating conditions. In the present device geometry (figure 14), over 80 % of the applied gate potential is estimated to fall across the gate oxide, justifying the use of a large gate-voltage increment. For each gate voltage, the I–V characteristics were measured between the drain (d) and source (s) electrodes, contacted by a 0.5µm radius coax probe (73Ct-CMIA/05), at a bias

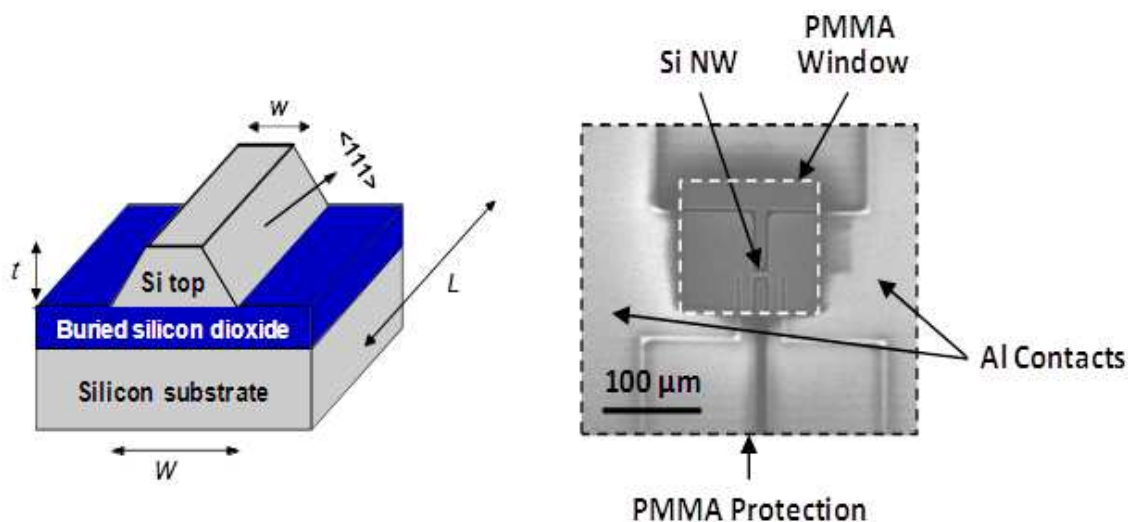range of between -6 V and +6 V, in 100-mV steps and/or from -0.2 to +0.2V in 4-mV steps, under ambient conditions.

Figure 14. In the right schematic the trapezoidal SiNW insulated from the silicon substrate by a buried SiO_2 layer is shown. The SiNWs used in this study have a length (L) of 1μm, a top width (w) of 70 nm, and a height (t) of 100 nm, The diagonal is based on (111) planes, whereas the small top is based on (100) plane. W (trapezoid base) =200 nm. The left image is a SEM image of the SiNW device, which is coated with PMMA protection layer.

5.1.1. Electrical effects of organic functionalities

Figure 15 shows the current–voltage characteristics of SiO_2-covered SiNW FETs and butyl-terminated SiNW FETs (as a representative example of the molecule-terminated SiNW FETs) at different gate voltages. The source–drain current (I_{sd}) of both samples increased with increasing gate voltage, indicating that the transport through the semiconducting SiNW is dominated by negative carriers (electrons), as it applies to the n-type SiNW. Figure 15 depicts tansconductance (g) versus back-gate voltage (V_g) in the SiO_2-SiNW-FET, butyl-SiNW-FET, 1,3-dioxan-2-ethyl-SiNW-FET, and propyl-alcohol-SiNW-FET. The data present-ed in figure 15 contain three distinctive features that seem to be at odds with one another and need to be explained. The first distinctive feature is an explicit dependence of the SiNW FET characteristics on the adsorbed molecules.

The zero-gate voltage (V_g=0), small-bias (V_{sd}=0–0.2V) tansconductance depends on the type of absorbed molecule. Particularly, one notices the following trend in the work function observed for these molecules (Table 4).: propyl-alcohol-SiNWs (0.5±0.1 μS)< SiO_2-SiNWs (2.8±0.4 μS) < allyl-SiNWs (7.3±0.8 μS)< butyl-SiNWs (7.6±0.9 μS) < 1,3-diox-an-2-ethyl-SiNWs (10.1±0.9 μS). Furthermore, the threshold voltage (V_{th}), which is roughly defined as the minimum gate voltage for the low-bias conductance to reach the saturation level (figure16) correlates well with the work function in freshly prepared 1,3-dioxan-2-ethyl, butyl and propyl-alcohol functionalities altering the V_{th} values to -4V,-2V, and+2V,respectively. These correlations seem to suggest that the influence of

the molecules on the operation of the SiNW FETs plays its most crucial role through a shift in the threshold gate voltage, as the effective work-function of the gate metal, or, equivalently, the electron affinity of the SiNW has been modified by introduction of the molecular layer. However, such a suggestion would be difficult to rationalize because the present molecular layer does not reside between the gate and the SiNW, but is located on the surface of the SiNW. Thus the molecular layer is not expected to directly shift the effective gate voltage [9]. Additionally, sign of the observed conductance shift is opposite to that of the expected work-function influence on the SiNW channel expected. For example, allyl, butyl, and 1,3-dioxan-2-ethyl functionalities are expected to impede the conduction through the Si channel because of the reduced Si electron affinity (see Table 4) but indeed an enhanced small-bias conductance was observed. In contrary to the distinctive feature for small gate-voltage characteristics, there are two other features concerning changes brought about by the adsorption of all the molecules. The first distinctive feature is the sizeable enhancement of the source–drain conductance at large, positive, gate voltages ($V_g > +3V$) from the one for SiO_2-SiNWs upon introduction of the molecules. However, this effect is almost independent of either the magnitude or the sign of work-function, essentially leading to the same curve as in figure 16. The second feature is that the tansconductance of the molecularly-terminated SiNW-FET devices are significantly reduced from that of the SiO_2-SiNWs at large negative gate bias ($V_g < -5V$). For SiO_2-SiNW FETs, the tansconductance decreases from 4.54 μS at Vg=+20 V only slightly to 1.47 μS at Vg=-20 V, indicating absence of on/off characteristics in this V_g region [9].

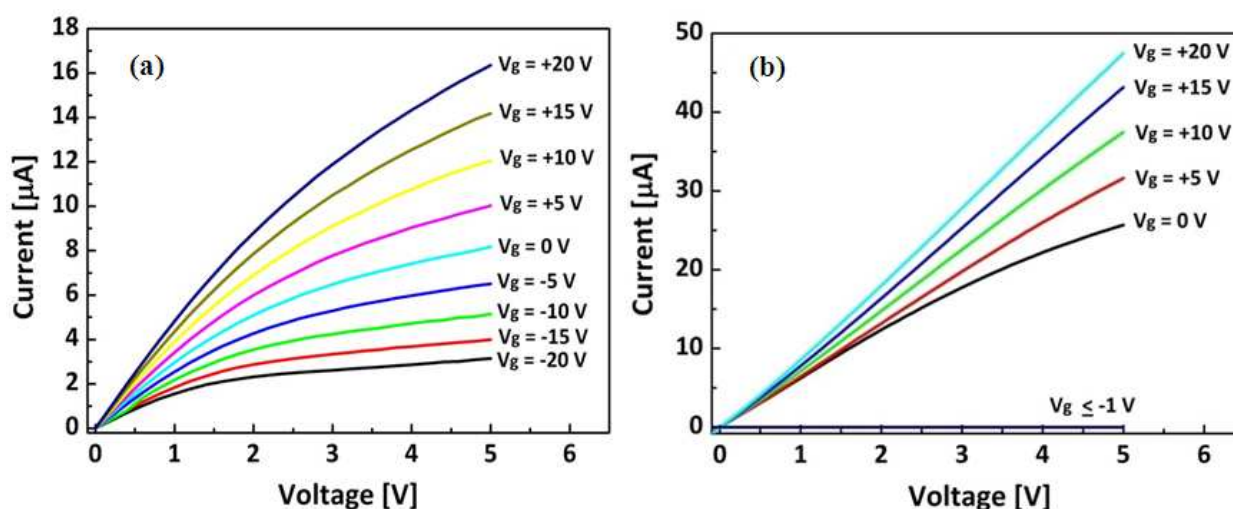**Figure 15.** I–V_{ds} curves of (a) SiO_2-SiNW FET (b) butyl-SiNW FET at different back-gate voltages (V_g)

With adsorption of molecules, the channel current is more effectively (by orders of magnitude) turned off by the negative gate voltage, resulting in a significant improvement in the on/off ratio of the FET device. Particularly, on/off ratios of $9x10^3$, $4x10^3$, and $1x10^2$ are observed for 1,3-dioxan-2-ethyl-, butyl-, and propyl-alcohol-terminated SiNW-FETs, respectively. Nevertheless,

it is worth to notice that models based on shifts in the threshold voltage from molecular dipolar layers are unable to explain the second and third characteristic observations.

Sample	work-function [meV]
Propyl-alcohol Si(111)	+500±50
SiO2-Si(111)	0±50
Allyl-Si(111)	-150±50
Butyl-Si(111)	-300±50
1,3-dioxan-2-ethyl-Si(111)	-400±50

Table 4. Change in work function due to molecule adsorption on Si(111) samples, as compared with SiO_2-Si(111). The measured work function of SiO_2-Si(111) samples was 4050 meV. The band banding was measured and found to be constant (80±5 meV) in all studied samples.
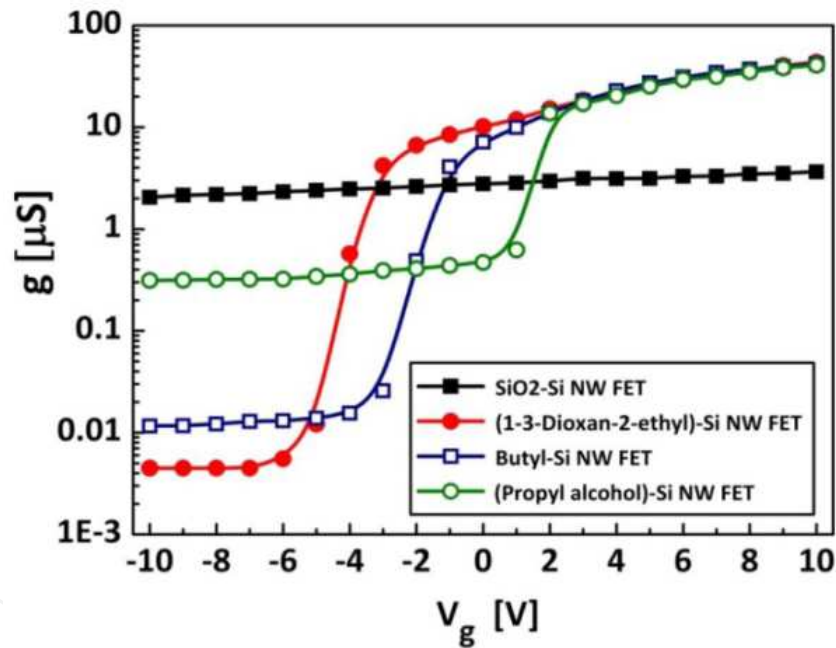

Figure 16. Tansconductance (g) versus back-gate voltage (V_g) in SiO_2-SiNW FET, butyl-SiNW FET, 1,3-dioxan-2-ethyl-SiNW FET, and propyl alcohol- SiNW FET. The tansconductance values were obtained at V_{sd}=0.2 V.

While the transistor characteristics for SiO_2-SiNW FETs have relative stability in air, properties of molecule-covered SiNW-FETs were found to evolve upon air exposure. The time dependence of the average tansconductance at V_g=0 V of various SiNWs versus time in air is illustrated in Fig.17, by a normalized parameter, namely γ (=g_t /$g_{t=0}$). For SiO_2-SiNWs, g is constant over the entire period of investigation. For both 1,3-dioxan-2-ethyl-SiNWs and butyl-SiNWs, g decreased with time to 30–40 % of its initial values over a period of one month (see figure 17). For SiNWs covered with propyl-alcohol, the observed decrease in g was more gradual.
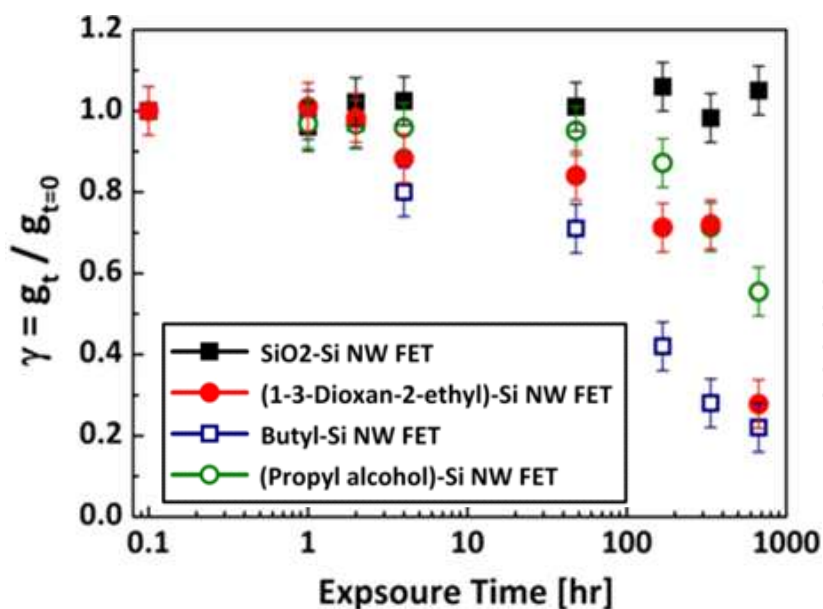
Figure 17. Normalized average conductance at V_g=0 of SiO_2-SiNW FET, butyl-SiNW FET, dioxan -propyl -SiNW FET, and propyl alcohol SiNW FET, versus air exposure time.

5.2. Photovoltaic cell based hybrid SiNWs

We compare three different surface terminations of SiNWs: (i) samples for which the oxide shell was removed by a standard HF dip, named H-SiNWs, (ii) samples with single monolayer of oxide grown after HF dip (14 days), shown by SiO_2-SiNWs; (iii) samples further processed by methyl functionalization immediately after the HF dip, marked with CH_3-SiNWs.
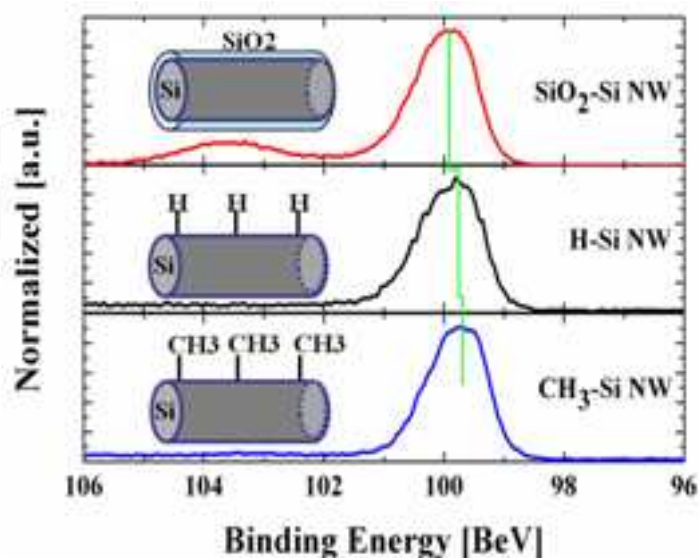

Figure 18. XP spectra of the Si2p region of SiO_2-SiNW, H-SiNW and CH_3-SiNW. The vertical solid line indicates the position of the chemically unshifted Si2p$_{3/2}$ component in each spectrum.

The observed binding energy of the $Si2p_{3/2}$ bulk signal allows determining the difference between the Fermi level and the energy of the valance-band maximum at the surface. We derive the binding energy of the Si2p signal with respect to the valance band maximum from the comparison between the Si 2p core level and valance band spectra of the three samples and obtain the value of $E_v-E_{Si2p3/2} = 98.72\pm0.02$ eV. This is similar to previous studies done by Himpsel et al [49] and Hunger et al. i.e. 98.74 eV [50]. Correspondingly, the data for E_F-E_V yields: 0.83 eV, 0.98 eV and 1.05 eV for CH$_3$-SiNW, H-SiNW and SiO$_2$-SiNW, respectively. The values yield slight downward surface band bending (B.B.) for the H-SiNW and SiO$_2$-SiNW and upward B.B for the CH$_3$-SiNW as will be discussed later.

5.2.1. Work function and band bending of the heterojunction

Work function of all the samples measured independently by the Kelvin probe method as $\Phi_{SiO2-SiNW}$= 4.32 eV, Φ_{H-SiNW}=4.26 eV, $\Phi_{CH3-SiNW}$=4.22 eV. Combining these data with the Fermi level position relative to the band edges (E_F-E_V), yields electron affinity values (χ) of 4.29 eV, 4.12 eV and 3.93 eV for SiO$_2$-SiNW, H-SiNW and CH$_3$-SiNW, respectively, according to $\chi= \Phi-E_g +(E_F-E_V)$. Summarizing these data, the band diagram depicted in figure 19 can be obtained. The bulk Fermi level position was obtained from the specific resistance (1-5 Ωcm) of the n-type samples and gave E_F-E_V=0.88$\pm$0.02 eV. We get a slight upward band bending of 0.05 eV which is consistent with flat band conditions for the CH$_3$-SiNW sample within our error margin. Identical results were found in photoemission studies on two dimensional methyl terminated Si(111) by Hunger et al. We get downward band bending corresponding to electron accumulation at the surface of the H-SiNW and SiO$_2$-SiNW. This uncommon aspect clearly indicates a yet unidentified surface doping process supporting the n-type character. As a tentative explanation, theory of Dittrich et al. can be referred that holds specific water based functional groups responsible for this effect [51]. For the SiO$_2$-SiNW, we add the band edges of the SiO$_2$ top layer and obtain almost a symmetric heterojunction with identical valance and conduction band discontinuities. With E_g=1.12 eV, estimating the electron affinity of the bulk silicon as 4.05 eV, the surface dipole, δ_{ss}, caused by the different monolayer surfaces were calculated to be +0.24 eV, +0.07 eV and -0.12 eV for SiO$_2$-SiNW, H-SiNW and CH$_3$-SiNW respectively. The surface dipoles are attributed to different bond charge distribution between the three samples.

5.2.2. Photoelectron Yield Spectroscopy (PYS)

The degree of surface band bending provides a measure for the quality of the electronic passivation on a semiconductor surface. Flat band conditions can usually be achieved only when surface defect states like dangling bonds are essentially passivated making them electronically inactive.

The improved electronic properties of the interface also influence directly the photoemission of electrons from the valance band edge and from surface states inside the band gap. These photoemission processes are studied by photoelectron yield spectroscopy (PYS).
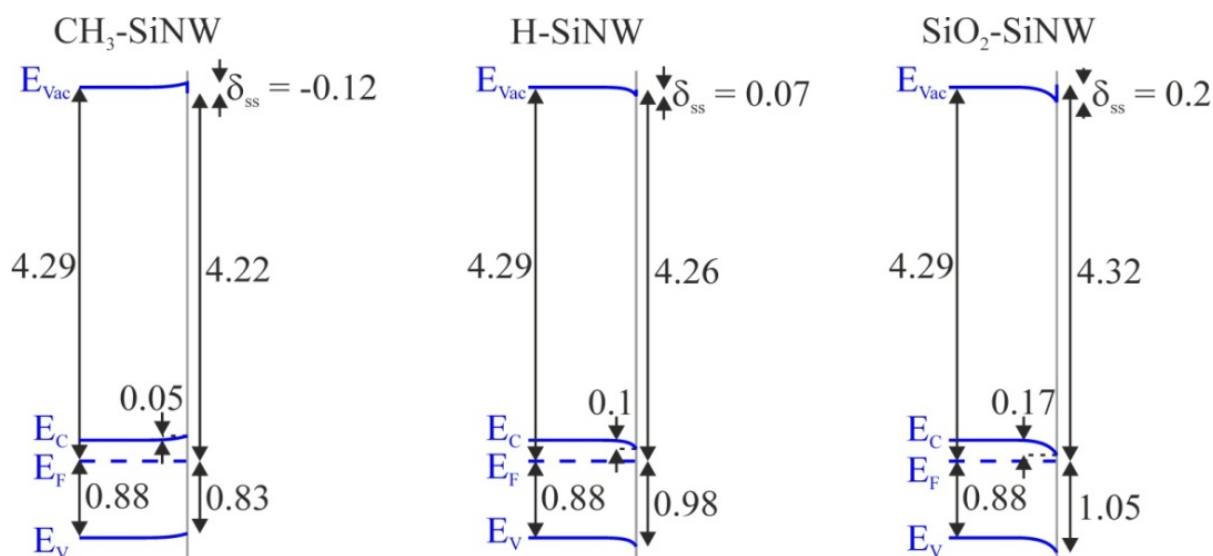
Figure 19. Surface energy band diagram of CH_3-SiNW, H-SiNW and SiO_2-SiNW surfaces. All the numbers are in eV units.

The photoelectron yield spectra of the three different NW samples investigated in this work are shown in figure 20. Each PY spectrum shows two thresholds near 5.0 ± 0.2 eV and 4.2 ± 0.2 eV. The higher energy band corresponds to the valence band density of states of the silicon while the lower energy band associates with defects in the band gap. These spectra essentially represent the occupied density of states. Since the reference energy for yield spectroscopy is the vacuum level (E_{Vac}), we independently used the work function data from the Kelvin measurements (E_{Vac}-E_F) to mark the spectral position of the Fermi level by the dotted vertical lines in figure 20.

The photoelectron intensity at lower photon energies compared to this level is due to thermal occupation of states beyond the Fermi level. The band edges of the two emissions were plotted by dashed lines as can be seen in figure 20. To this end, we can distinguish between the two emissions, for example, the CH_3 show higher emission of 10^2 at 4.7 eV (note the logarithmic scale). Obviously the ratio between defect states and valence band states is significantly different for the three samples. For a systematic comparison we have redrawn the yield spectra in figure 21. The top energy axes in those plots are now related to the valence band maximum instead of the vacuum level by using the electron affinities of the three samples (see figure 21) and the band gap energy of silicon.

The spectra are further normalized at the energy of 0.76 eV below the valence band maximum where they should be strongly dominated by the valence band emission only and thus, the PYS should be identical for all the three samples at this energy point (See figure 21). By this procedure, the relative defect contributions are scaled for all three samples to the Si valence band density of states and are better comparable. The highest defect density is seen for the SiO_2-SiNWs and in this case the defect and the valence band emissions are hardly resolved as two different bands (see also figure 21a).

In the case of the H-SiNW, the defect band is already lower by a factor of about 2, and it can be well distinguished from the valence band emission. Finally, the lowest defect density is observed for the CH₃-SiNWs. For this sample, however, a third band between 4.7 and 5.3 eV is clearly visible and can be distinguished by a significantly smaller slope of the spectrum in this energy region compared to the spectra of the other two samples.
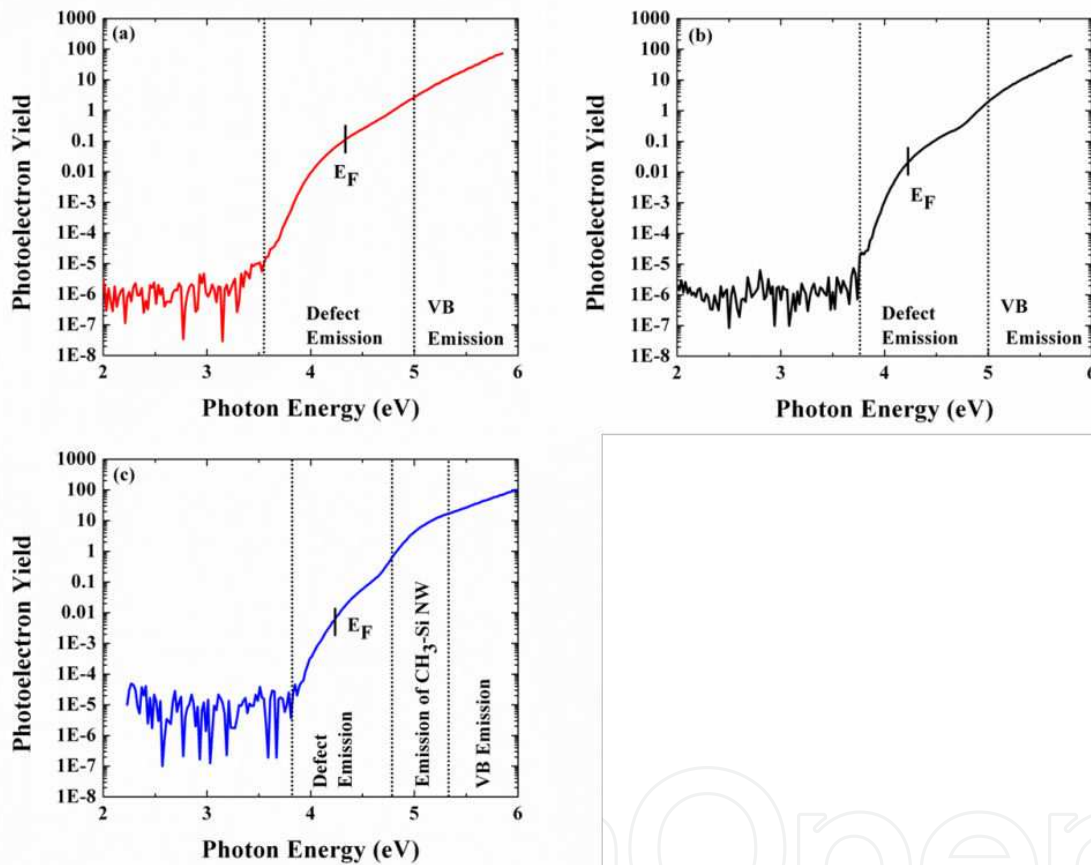

Figure 20. Photoemission yield spectrum of (a) SiO_2-SiNW, (b) H-SiNW, (c) CH_3-SiNW.

This additional band is even more obvious in the spectroscopic density of states that is a derivative of the yield spectra, as shown in figure 21b. Microscopic origin of this additional photoemission band which is presumably related to the methyl functionalization is not yet clear and is subject of further investigations. It is noteworthy to mention that the bandgap energies for SiO_2-SiNWs and CH_3-SiNWs are ~8.9 eV and 7.3 eV, respectively [52]. These values notably differ and thus elucidate the importance of the surface termination with molecules for any electronic application of NWs.
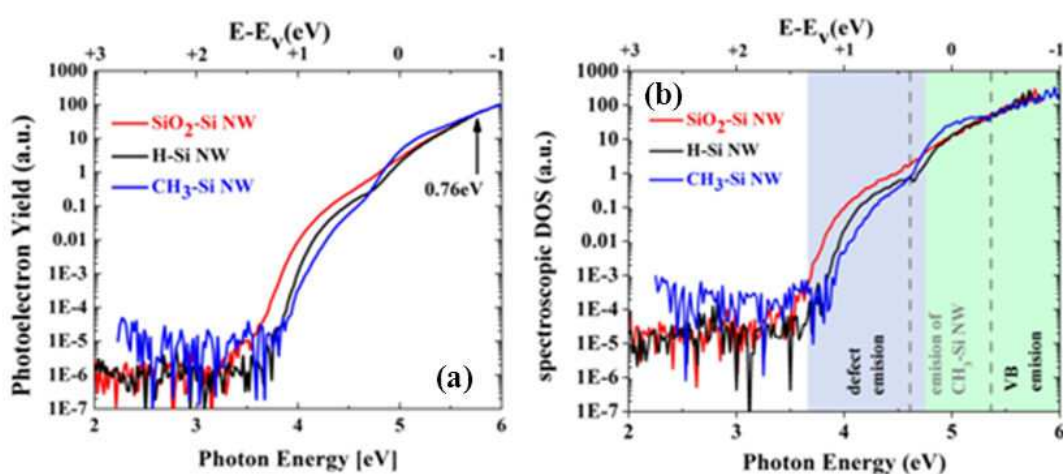
Figure 21. Photoelectron yield Y(hv) spectra and spectroscopic density of states of SiO$_2$-SiNW, H-SiNW and CH$_3$-SiNW.

5.2.3. I-V curves of solar cells processed with functionalized SiNWs

Here we demonstrate a hybrid organic / inorganic solar cell based on a combination of a polymer (PEDOT:PSS) constituting the hole conductor and SiNWs play the role of light absorber and electron conductor. NWs employed to assemble the photovoltaic cells are synthesized on the basis of metal-assisted etching rather than VLS growth. Solar cell performance differs between cells of SiNWs with various functionalities [53].

Surfaces of those SiNWs were terminated by H-, SiO$_2$- and CH$_3$- and integrated into a solar cell through identical processes. In all the cells the photogenerated electron-hole pairs are separated at a heterojunction which forms at the SiNW/polymer interface (see figure 22a). The H-SiNWs can just be excluded from further solar cell studies due to the fact that such surfaces indicate hydrophobic behavior and the spun polymer does not wet the SiNW properly.

This hybrid solar cell concept follows the principle proposed by Lewis et al. [54] who made use of the advantageous separation in orthogonal directions of light absorption in the SiNWs and charge carrier separation at the wrap around heterojunction. This SiNW-based cell concept has the following advantages: (i) efficient absorption of light in SiNWs [55] (ii) short diffusion distance for carriers to the wrapped around heterojunction; (iii) use of the air-stable and robust polymer, PEDOT:PSS, as an efficient hole conductor; (iv) the SiNW/ polymer solar cell design utilizes only 1 % of Si used in thin film cells of identical thicknesses. However, for photovoltaic application full coverage of SiNWs by PEDOT:PSS is desirable but not yet achieved (approximately 320nm was covered on top SiNW edge as can be seen in figure 22a.

SiNWs serve mainly as light trapping structures; reduce diffusion distance to the nanowires length while uncovered surfaces represent recombination centers for charge carriers. Further studies on wetting agents added to PEDOT:PSS may result in full coverage and higher efficiencies. Figure 22b shows the current density-voltage (J-V) characteristics of CH$_3$-SiNW/ PEDOT:PSS and SiO$_2$-SiNW/PEDOT:PSS solar cells under AM1.5 illumination. SiO$_2$-SiNW/ PEDOT:PSS samples bear a short circuit current (J_{sc}) of 1.6mA/cm^2, an open circuit voltage

(V_{oc}) of 320 mV, a fill factor (*FF*) of 0.53 and a conversion efficiency (η) of 0.28 %. CH$_3$-SiNW/ PEDOT:PSS devices exhibit improved performance with J_{sc}, V_{oc}, *FF* and μ magnitudes of 7.0 mA/cm^2, 399 mV, 0.44 and 1.2 %, respectively. The low values of FF and J_{sc} in both types of samples are attributed to high contact resistances (Rs 300Ω).

It should be noted that by decreasing the resistance we can improve the efficiency of the so-lar cell as shown by different groups [56-58]. In spite of notably low efficiencies relative to the values nowadays reported for efficient solar cells, their comparative increase (of about a factor of 4) upon methylation that proves a very promising prospective for this kind of sur-face functionalization.

The improved performance of the CH$_3$-SiNWs is attributed to the removal of the tunnelling oxide and the reduction of defect states related PY which is caused by a reduced defect den-sity at the heterojunction interface. The advantage of methyl functionalization for the solar cell application has more aspects. The negative surface dipole polarity (-0.12 eV) of the CH$_3$-SiNW leads to a favorable barrier formation between Si and PEDOT:PSS. Lewis et al. report that charge transfer rates for CH$_3$-Si do not differ from those of H-Si so that CH$_3$-monolayers represent no appreciable tunneling barrier for charge transfer at room temperature [59].

Moreover, using one monolayer of CH$_3$ at the interface, allow a more efficient charge cou-pling between silicon and polymer. By reducing the defect density at CH$_3$-SiNWs (see PYS section), the surface recombination is decreased and cause an improvement in V_{oc}. Accord-ing to the Shockley diode equation $V_{oc} = k_BT/q \cdot \ln(J_{sc}/J_0)$, where J_0 is the saturation current and the other variables have their usual meanings. Since increase of J_{sc} influences V_{oc} as well, it has to be mentioned that the V_{oc} gain observed cannot rely on this effect alone.

Assuming a similar J_0, which correspond to the removal of the tunneling oxide without changing the interface properties, the increase of J_{sc} would lead to a V_{oc} gain of $\Delta V_{oc} = kT/q \cdot \ln(J_{sc,methyl}/J_{sc,oxide}) = k_BT/q \cdot \ln(7.0/1.6) = 0.037$ V. Regarding the observed gain of $\Delta V_{oc} = 0.079$ V, only a reduced surface recombination (as measured by PY) and/or a favorable barrier forma-tion (surface dipole) can establish consistency with the experimental data.
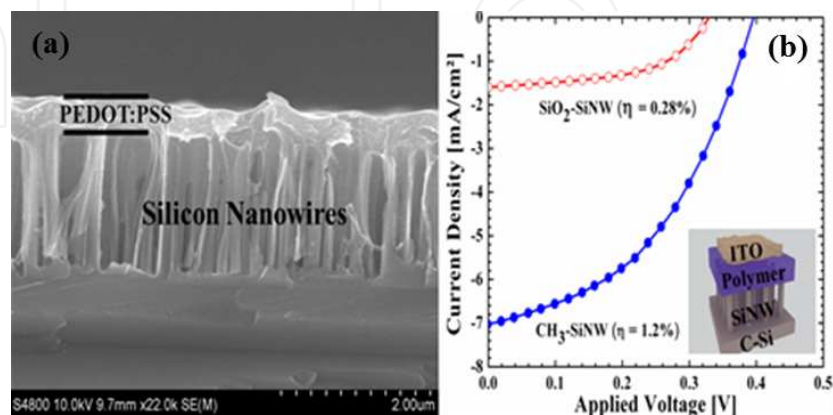

Figure 22. (a) Tilted view of the heterojunctionSiNW/PEDOT:PSS. (b) J-V characteristic under AM1.5 illuminations of the radial heterojunction solar cells from CH$_3$-SiNW and SiO$_2$-SiNW. Inset: schematic view of solar cell device structure.

A potential explanation of the increase in the PY of CH_3-SiNW and an increased efficiency of processed solar cells could be that CH_3-SiNWs simply absorb the solar light better than the other SiNW. This can experimentally falsified by the equal total absorbance (A), reflection (R) and transmission (T) of all three types of samples (see figure 23.

All the three spectra (SiO_2-SiNW, CH_3-SiNW, H-SiNW) show the same basic structure and the same A, R, T in short wavelengths (hv > E_g). In wavelengths smaller than ~1000 nm, the three samples behave the same: reflection is around 10 %, the transmission is roughly 0 % and thus the absorption around 90 % for the whole visible spectrum. This tendency is observed even in multi monolayers of oxide. However, for wavelengths larger than ~1200 nm (attribute to surface state regime) the transmission is around 50 % for all three samples and the reflection is also nearly 50 %, except for the SiO_2-SiNW sample which shows 40 %. The lower reflection in SiO_2-SiNW is attributed to light adsorption of the surface state.
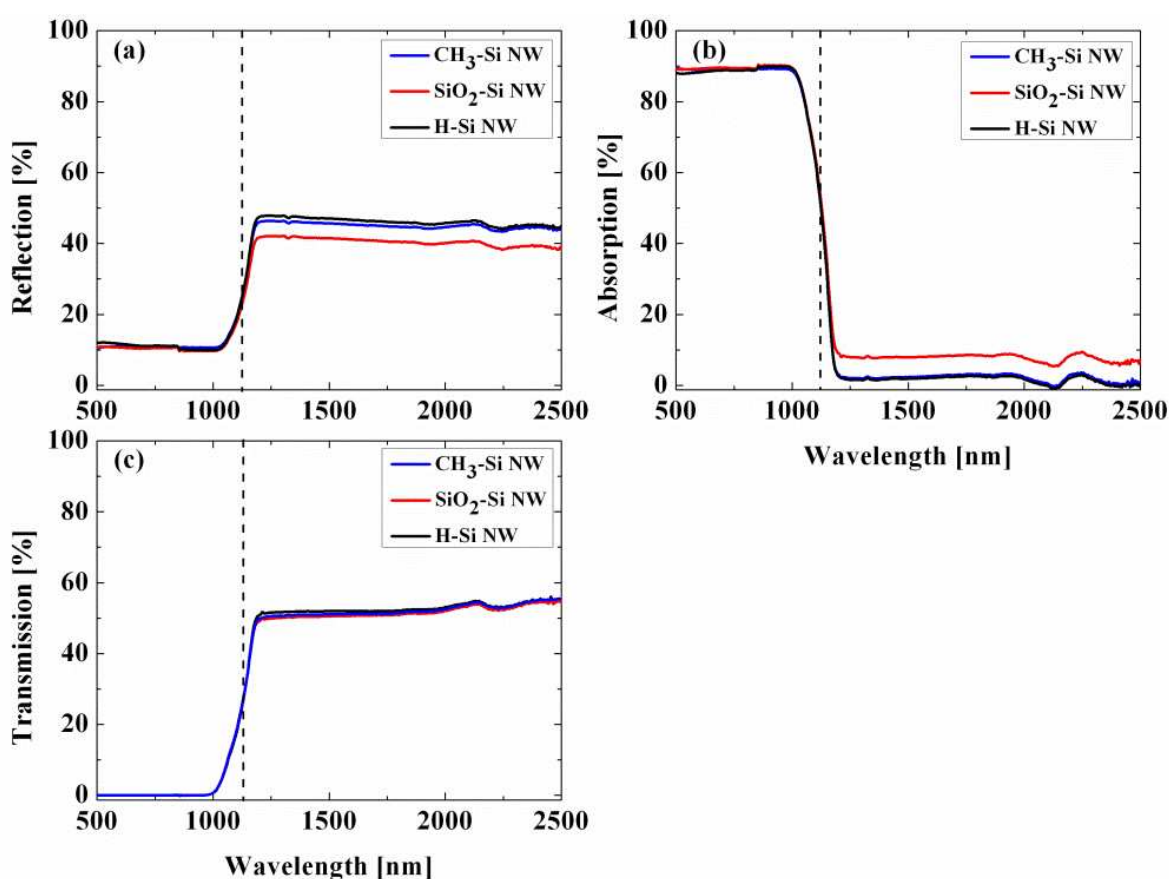

Figure 23. Spectra of SiO_2-SiNW, H-SiNW and CH_3-SiNW: (A) Reflectance (B) Transmission (C) absorbance. The dash line indicates the wavelength that corresponds to the SiNW band gap energy.

In summary, we terminated the SiNWs with organic molecules. The stability of the organic found to be depended on their coverage and surface. CH_3 shows the highest oxide resistivity, since it gives 100 % of coverage. To utilize the advantage of these molecules, we integrate them in FETs and solar cells. We showed that we can tune the properties of the FETs by at-

taching molecules on the surface of the channel i.e. SiNW. The solar cells of hybrid SiNW shows higher efficiency than native oxide. This can be attributed to the low defects in the band gap as had been shown by photoelectron yield spectra.

Author details

Muhammad Y. Bashouti[1], Matthias Pietsch[1], Kasra Sardashti[1], Gerald Brönstrup[1], Sebastian W. Schmitt[1], Sanjay K. Srivastava[1], Jürgen Ristein[3], Jordi Arbiol[4], Hossam Haick[2] and Silke Christiansen[1,5]

1 Max-Planck-Institute for the Science of Light, Erlangen, Germany

2 The Department of Chemical Engineering and Russell Berrie Nanotechnology Institute, Technion – Israel Institute of Technology, Haifa, Israel

3 Institue for Technical Physics, University of Erlangen-Nuremberg, Erlangen, Germany

4 Institució Catalana de Recerca i EstudisAvançats (ICREA) and Institut de Ciència de Materials de Barcelona,ICMAB-CSIC, Bellaterra, Spain

5 Institute of Photonic Technology, Jena, Germany

References

[1] Bandaru, P.R. and P. Pichanusakorn, *An outline of the synthesis and properties of silicon nanowires.* Semiconductor Science and Technology, 2010. 25(2).

[2] Assad, O., et al., *Stable Scaffolds for Reacting Si Nanowires with Further Organic Functionalities while Preserving Si-C Passivation of Surface Sites.* Journal of the American Chemical Society, 2008. 130(52): p. 17670-+.

[3] Barth, S., et al., *Synthesis and applications of one-dimensional semiconductors.* Progress in Materials Science, 2010. 55(6): p. 563-627.

[4] Bronstrup, G., et al., *Statistical model on the optical properties of silicon nanowire mats.* Physical Review B, 2011. 84(12).

[5] Paska, Y., et al., *Enhanced Sensing of Nonpolar Volatile Organic Compounds by Silicon Nanowire Field Effect Transistors.* Acs Nano, 2011. 5(7): p. 5620-5626.

[6] Paska, Y. and H. Haick, *Interactive Effect of Hysteresis and Surface Chemistry on Gated Silicon Nanowire Gas Sensors.* Acs Applied Materials & Interfaces, 2012. 4(5): p. 2604-2617.

[7] Bashouti, M.Y., et al., *Chemical Passivation of Silicon Nanowires with C(1)-C(6) Alkyl Chains through Covalent Si-C Bonds.* Journal of Physical Chemistry C, 2008. 112(49): p. 19168-19172.

[8] Bashouti, M.Y., et al., *Covalent Attachment of Alkyl Functionality to 50 nm Silicon Nanowires through a Chlorination/Alkylation Process.* Journal of Physical Chemistry C, 2009. 113(33): p. 14823-14828.

[9] Bashouti, M.Y., R.T. Tung, and H. Haick, *Tuning the Electrical Properties of Si Nanowire Field-Effect Transistors by Molecular Engineering.* Small, 2009. 5(23): p. 2761-2769.

[10] Paska, Y. and H. Haica, *Controlling properties of field effect transistors by intermolecular cross-linking of molecular dipoles.* Applied Physics Letters, 2009. 95(23).

[11] Qiu, T. and P.K. Chu, *Self-selective electroless plating: An approach for fabrication of functional 1D nanomaterials.* Materials Science & Engineering R-Reports, 2008. 61(1-6): p. 59-77.

[12] Chen, W.W., et al., *Etching Behavior of silicon nanowires with HF and NH4F and surface characterization by attenuated total reflection Fourier transform infrared spectroscopy: Similarities and differences between one-dimensional and two-dimensional silicon surfaces.* Journal of Physical Chemistry B, 2005. 109(21): p. 10871-10879.

[13] Chan, C.K., et al., *High-performance lithium battery anodes using silicon nanowires.* Nature Nanotechnology, 2008. 3(1): p. 31-35.

[14] Chen, L.J., *Silicon nanowires: the key building block for future electronic devices.* Journal of Materials Chemistry, 2007. 17(44): p. 4639-4643.

[15] Cui, Y. and C.M. Lieber, *Functional nanoscale electronic devices assembled using silicon nanowire building blocks.* Science, 2001. 291(5505): p. 851-853.

[16] Cui, Y., et al., *High performance silicon nanowire field effect transistors.* Nano Letters, 2003. 3(2): p. 149-152.

[17] Goldberger, J., et al., *Silicon vertically integrated nanowire field effect transistors.* Nano Letters, 2006. 6(5): p. 973-977.

[18] Peng, K.Q., et al., *Silicon nanowires for rechargeable lithium-ion battery anodes.* Applied Physics Letters, 2008. 93(3).

[19] Haick, H., et al., *Electrical characteristics and chemical stability of non-oxidized, methyl-terminated silicon nanowires.* Journal of the American Chemical Society, 2006. 128(28): p. 8990-8991.

[20] Morales, A.M. and C.M. Lieber, *A laser ablation method for the synthesis of crystalline semiconductor nanowires.* Science, 1998. 279(5348): p. 208-211.

[21] Ashkenasy, G., et al., *Molecular engineering of semiconductor surfaces and devices.* Accounts of Chemical Research, 2002. 35(2): p. 121-128.

[22] Cohen, R., et al., *Molecular electronic tuning of Si surfaces.* Chemical Physics Letters, 1997. 279(5-6): p. 270-274.

[23] Ishii, H., et al., *Energy level alignment and interfacial electronic structures at organic/metal and organic/organic interfaces (vol 11, pg 605, 1999).* Advanced Materials, 1999. 11(12): p. 972-972.

[24] Anagaw, A.Y., R.A. Wolkow, and G.A. DiLabio, *Theoretical study of work function modification by organic molecule-derived linear nanostructure on H-silicon(100)-2 x 1.* Journal of Physical Chemistry C, 2008. 112(10): p. 3780-3784.

[25] Hiremath, R.K., et al., *Molecularly controlled metal-semiconductor junctions on silicon surface: A dipole effect.* Langmuir, 2008. 24(19): p. 11300-11306.

[26] Aradi, B., et al., *Theoretical study of the chemical gap tuning in silicon nanowires.* Physical Review B, 2007. 76(3).

[27] Leu, P.W., B. Shan, and K.J. Cho, *Surface chemical control of the electronic structure of silicon nanowires: Density functional calculations.* Physical Review B, 2006. 73(19).

[28] Wagner, R.S., et al., *Study of Filamentary Growth of Silicon Crystals from Vapor.* Journal of Applied Physics, 1964. 35(10): p. 2993-&.

[29] Sivakov, V.A., et al., *Silicon nanowire oxidation: the influence of sidewall structure and gold distribution.* Nanotechnology, 2009. 20(40).

[30] Bashouti, M.Y., et al., *Silicon nanowires terminated with methyl functionalities exhibit stronger Si-C bonds than equivalent 2D surfaces.* Physical Chemistry Chemical Physics, 2009. 11(20): p. 3845-3848.

[31] Haber, J.A. and N.S. Lewis, *Infrared and X-ray photoelectron spectroscopic studies of the reactions of hydrogen-terminated crystalline Si(111) and Si(100) surfaces with Br-2, I-2, and ferrocenium in alcohol solvents.* Journal of Physical Chemistry B, 2002. 106(14): p. 3639-3656.

[32] Thanikasalam, P., T.K. Whidden, and D.K. Ferry, *Oxidation of silicon (100): Experimental data versus a unified chemical model.* Journal of Vacuum Science & Technology B, 1996. 14(4): p. 2840-2844.

[33] Dimitrijev, S. and H.B. Harrison, *Modeling the growth of thin silicon oxide films on silicon.* Journal of Applied Physics, 1996. 80(4): p. 2467-2470.

[34] Deal, B.E. and A.S. Grove, *General Relationship for Thermal Oxidation of Silicon.* Journal of Applied Physics, 1965. 36(12): p. 3770-&.

[35] Liu, B.Z., et al., *Oxidation of silicon nanowires for top-gated field effect transistors.* Journal of Vacuum Science & Technology A, 2008. 26(3): p. 370-374.

[36] Buttner, C.C. and M. Zacharias, *Retarded oxidation of Si nanowires.* Applied Physics Letters, 2006. 89(26).

[37] Miyazaki, S., et al., *Surface Fermi level position of hydrogen passivated Si(111) surfaces.* Applied Physics Letters, 1996. 68(9): p. 1247-1249.

[38] Cerofolini, G.F., G. LaBruna, and L. Meda, *Gas-phase room-temperature oxidation of (100) silicon.* Applied Surface Science, 1996. 93(3): p. 255-266.

[39] Cerofolini, G.F. and L. Meda, *Mechanisms and kinetics of room-temperature silicon oxidation.* Journal of Non-Crystalline Solids, 1997. 216: p. 140-147.

[40] Reddy, S., P.O. Assad, and H. Haick, *Highly stable organic modification of Si(111) surfaces: Towards reacting Si with further functionalities while preserving the desirable chemical properties of full Si-C atop site terminations.* Journal of the American Chemical Society, 2008. 130(29): p. 9184-+.

[41] Cerofolini, G.F., D. Mascolo, and M.O. Vlad, *A model for oxidation kinetics in air at room temperature of hydrogen-terminated (100) Si.* Journal of Applied Physics, 2006. 100(5).

[42] Uematsu, M., H. Kageshima, and K. Shiraishi, *Microscopic mechanism of thermal silicon oxide growth.* Computational Materials Science, 2002. 24(1-2): p. 229-234.

[43] Ma, D.D.D., et al., *Small-diameter silicon nanowire surfaces.* Science, 2003. 299(5614): p. 1874-1877.

[44] Zhang, R.Q., et al., *Structures and energetics of hydrogen-terminated silicon nanowire surfaces.* Journal of Chemical Physics, 2005. 123(14).

[45] Sun, X.H., et al., *FTIR spectroscopic studies of the stabilities and reactivities of hydrogen-terminated surfaces of silicon nanowires.* Inorganic Chemistry, 2003. 42(7): p. 2398-2404.

[46] Wallart, X., C.H. de Villeneuve, and P. Allongue, *Truly quantitative XPS characterization of organic monolayers on silicon: Study of alkyl and alkoxy monolayers on H-Si(111).* Journal of the American Chemical Society, 2005. 127(21): p. 7871-7878.

[47] Schwartz, D.K., *Mechanisms and kinetics of self-assembled monolayer formation.* Annual Review of Physical Chemistry, 2001. 52: p. 107-137.

[48] Nuzzo, R.G., B.R. Zegarski, and L.H. Dubois, *Fundamental-Studies of the Chemisorption of Organosulfur Compounds on Au(111) - Implications for Molecular Self-Assembly on Gold Surfaces.* Journal of the American Chemical Society, 1987. 109(3): p. 733-740.

[49] Himpsel, F.J., G. Hollinger, and R.A. Pollak, *Determination of the Fermi-Level Pinning Position at Si(111) Surfaces.* Physical Review B, 1983. 28(12): p. 7014-7018.

[50] Hunger, R., et al., *Chemical and electronic characterization of methyl-terminated Si(111) surfaces by high-resolution synchrotron photoelectron spectroscopy.* Physical Review B, 2005. 72(4).

[51] Dittrich, T., et al., *On the origin of the positive charge on hydrogenated Si surfaces and its dependence on the surface morphology.* Surface Science, 1999. 437(1-2): p. 154-162.

[52] Salomon, A., et al., *What is the barrier for tunneling through alkyl monolayers? Results from n- and p-Si-Alkyl/Hg junctions.* Advanced Materials, 2007. 19(3): p. 445-+.

[53] Sivakov, V., et al., *Silicon Nanowire-Based Solar Cells on Glass: Synthesis, Optical Properties, and Cell Parameters.* Nano Letters, 2009. 9(4): p. 1549-1554.

[54] Boettcher, S.W., et al., *Energy-Conversion Properties of Vapor-Liquid-Solid-Grown Silicon Wire-Array Photocathodes.* Science, 2010. 327(5962): p. 185-187.

[55] Bronstrup, G., et al., *A precise optical determination of nanoscale diameters of semiconductor nanowires.* Nanotechnology, 2011. 22(38).

[56] Ozdemir, B., et al., *Silicon nanowire - poly(3,4-ethylenedioxythiophene)-poly(styrenesulfonate) heterojunction solar cells.* Applied Physics Letters, 2011. 99(11).

[57] Yuan, C.Z., et al., *Hierarchically structured carbon-based composites: Design, synthesis and their application in electrochemical capacitors.* Nanoscale, 2011. 3(2): p. 529-545.

[58] Shiu, S.C., et al., *Morphology Dependence of Silicon Nanowire/Poly(3,4-ethylenedioxythiophene):Poly(styrenesulfonate) Heterojunction Solar Cells.* Chemistry of Materials, 2010. 22(10): p. 3108-3113.

[59] Maldonado, S. and N.S. Lewis, *Behavior of Electrodeposited Cd and Pb Schottky Junctions on CH3-Terminated n-Si(111) Surfaces.* Journal of the Electrochemical Society, 2009. 156(2): p. H123-H128.